

Major Nutrient Fronts in the Northeastern Atlantic: From the Subpolar Gyre to Adjacent Shelves



Hjálmar Hátún, Karin Margretha H. Larsen, Sólva Káradóttir Eliassen, and Moritz Mathis

Contents

| | | |
|-----|---|-----|
| 1 | Introduction | 98 |
| 2 | Nutrient Fronts in the Open Ocean | 101 |
| 2.1 | The Main Thermocline: Currents and Water Masses | 101 |
| 2.2 | From the Thermocline to the Photic Zone | 102 |
| 2.3 | The Subpolar Gyre | 104 |
| 2.4 | On and Around Rockall | 106 |
| 2.5 | The Iceland Basin | 110 |
| 2.6 | An Integrated Perspective: In the Context of Sea-Surface Height, MLD, and the Gyre Index | 115 |
| 2.7 | After Established Summer Stratification | 117 |
| 3 | Onwelling to Adjacent Shelves | 122 |
| 3.1 | From the Northeast Atlantic to the North Sea | 122 |
| 3.2 | The Faroe Shelf | 126 |
| 4 | Summary | 133 |
| | References | 135 |

Abstract Diatom-dominated spring blooms in the northeastern Atlantic, both in the open ocean and on adjacent shelves, become silicate-limited every spring/summer. We here review the fertilizing silicate fluxes from the large subpolar gyre source, across the major oceanic Subarctic Front and further across shelf edge and tidal mixing fronts and onto adjacent shelves. As a case study, we illustrate potential linkages between the open ocean dynamics and the primary production, fish larvae

H. Hátún (✉), K. M. H. Larsen, and S. K. Eliassen
Faroe Marine Research Institute, Tórshavn, Faroe Islands
e-mail: hjalmarh@hav.fo; karinl@hav.fo; solvae@hav.fo

M. Mathis
Max Planck Institute for Meteorology, Hamburg, Germany
e-mail: moritz.mathis@hzg.de

abundances and seabird breeding success within the Faroe shelf ecosystem. The “boosting effect” of vigorous winter convection occurring every 5–8 years is illustrated, and we also discuss the pre-bloom silicate decline, which has taken place throughout the entire subpolar North Atlantic since the early 1990s. Reduced winter convection due to global warming is projected by most climate models, and this is expected to have severe impact on the North Atlantic Ocean primary production.

Keywords Lateral exchange, Mixed layer depth, Productivity, Silicate, Subpolar gyre

1 Introduction

The open ocean boreal waters in the northeastern Atlantic host some of the largest pelagic fish stocks in the world [1], and the adjacent continental shelves support rich marine ecosystems – including commercially important fish stocks [2] and large seabird colonies [3, 4]. There is a growing recognition of how climate variability and large-scale oceanography can regulate both the biomass and regional distribution of these important marine resources. However, establishing possible climate-ecosystem linkages has been generally limited to the utilization of sea temperatures as an environmental proxy [5, 6], without much consideration for nutrient dynamics.

Nutrient limitation of primary production at lower latitudes is “textbook knowledge” [7], but the oceanographic community has often overlooked the likely importance of this fundamental ecosystem driver in boreal/subarctic parts of the North Atlantic Ocean. Only very few studies have investigated possible linkages between ocean dynamics and nutrient concentrations there. The subpolar North Atlantic is characterized by strong spring blooms [8, 9]. These generally ensue after positive air-sea heat fluxes stratify the near-surface layer around April–May, although several other hypotheses for the bloom initiation have been proposed ([10] – and references therein). These blooms consist primarily of diatoms, which are fast-growing algae that, in addition to phosphate and nitrate, require silicate to sustain their growth [11, 12]. Macronutrients are quickly drawn out of the shallow summer mixed layer, and in the North Atlantic, silicate typically becomes the limiting nutrient for diatom growth [11, 13] – occasionally confounded by seasonal iron limitation [14]. After this, new production becomes restricted to upwelling regions, e.g., along the large-scale nutrient fronts and along the continental slopes [11]. Diatoms are an important food source for secondary producers, and in particular for calanoid copepods such as *Calanus finmarchicus*, which itself is a key prey item linking phytoplankton to higher trophic levels in subpolar ecosystems [15]. Predators like pelagic fish and seabirds will therefore congregate at such upwelling feeding hotspots during summer [16–18].

However, the processes through which the larger basin scale could alter the productivity along fronts are not well understood. If rectified supply of nutrients is the dominant process and involves vertical transfer near fronts [11], then this raises the question of how the underlying nutrients in the thermocline are maintained. Without a continuous supply to the thermocline, any near-front rectified supply will only provide an initial enhancement in productivity. This will gradually decrease in time until an equilibrium state is reached at lower productivity. One task is therefore to trace the supply of nutrients in the deeper waters.

The northeastern (NE) Atlantic receives a mix of nutrient-poor subtropical waters from the Bay of Biscay and the Gulf Stream, and a contrasting nutrient-rich subarctic water contribution from the subpolar gyre (SPG, a list of acronyms is provided in Table 2) in the west [19] (Fig. 1). Strong nutrient gradients are co-located with the Subarctic Front (SAF), which divides the subtropical and subarctic water masses – and which thus outlines the main periphery of the SPG.

The NE Atlantic encompasses the confluence of these contrasting water masses. Consequently the nutrient dynamics within this region are highly sensitive to the strength and size of the subpolar gyre [22, 24, 26] and lateral shifts of the SAF (Fig. 1b) – the large-scale *nutrient front*. However, in order to fertilize the poleward flowing Atlantic waters, subarctic waters of the SPG must be transported across the SAF. The SAF is a three-dimensional structure (Fig. 1e), therefore the cross-frontal transport also has a vertical dimension. Strong nutrient gradients are located at the base of the winter mixed layer, separating the nutrient-poor Atlantic waters from nutrient-rich waters below. The nutrient concentrations off the south Iceland and European continental slopes are therefore regulated by the SAF dynamics and the winter convection – both associated with the dynamics of the SPG [26, 27] – as well as the summer mixed layer dynamics [28].

Further north, in the southern Norwegian Sea, the northward flowing Atlantic water meets southeastward flowing subarctic waters from the Greenland and Iceland Seas. This establishes the Iceland-Faroe Front (IFF) (Fig. 1b) – another large-scale nutrient front [11]. The Atlantic waters surrounding the Faroe shelf are influenced by the IFF dynamics, in addition to the upstream SPG regulation and the strength of the summer mixed layer.

The ecosystems of the adjacent European, south Iceland and Faroe shelves are critically dependent on nutrient fluxes from the open ocean [29, 30], since riverine nutrient input only enriches the very near-coast band along these seaboards. This ocean-to-shelf *onwelling* of nutrients [31] requires cross-frontal exchanges (shelf edge fronts along the margins and tidal mixing fronts in shallower waters, Fig. 1b) in order to bring nutrients from the open ocean onto the shelves [28, 32].

In this chapter, we illustrate the nutrient pathway from the North Atlantic SPG, across open-ocean nutrient fronts and slope fronts, to adjacent shelves. Emphasis is put on silicates and the Faroe shelf ecosystem. This should not be regarded as a complete review, but rather a story which builds on some selected and relevant publications, complemented by more general reviews of important sub-topics. In Sect. 2, we describe the large-scale open-ocean nutrient fronts and other basic SPG-related oceanographic features, which could be important for the pre-bloom

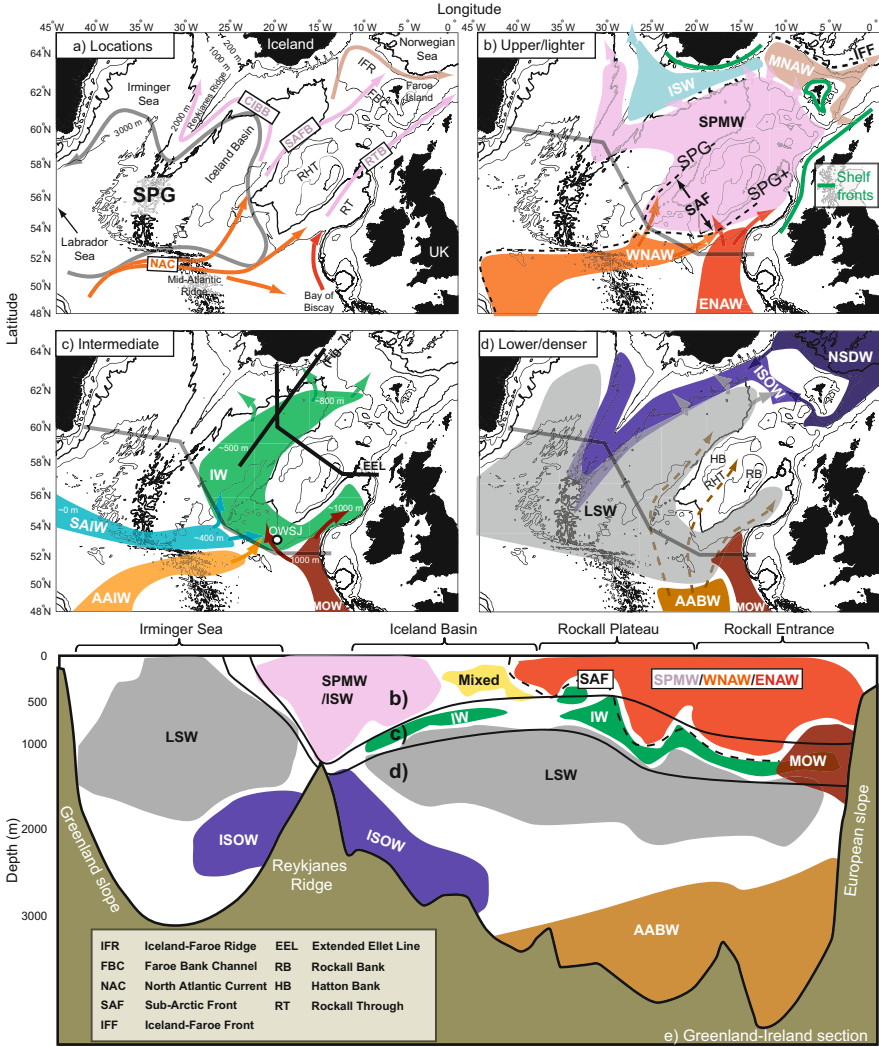


Fig. 1 Overview. (a) Bathymetry, toponyms, the approximate outline of the subpolar gyre (SPG, gray) and the main Atlantic inflows current branches (reddish arrows). A vertical view of main water masses along the AIE WOCE section from Greenland to Ireland (gray line in panels b, c and d) is shown in (e). This is based on the occupation of this section in 1991, presented in [20]. The rough horizontal distribution of the water masses is illustrated by vertically dividing them into an upper/lighter layer (b), an intermediate layer aligned with the permanent pycnocline (c), and a deeper/denser layer (d). The approximate position of the oceanic Sub-Arctic Front (SAF) is illustrated with black dashed lines (b and e) and differentiated between a strong subpolar gyre state (SPG+) and a weak state (SPG-, respectively in panel (b)). Near-shelf fronts are also sketched (green in b). The black lines in (c) show the sections presented in Figs. 5, 7, and 8. The water mass acronyms are summarized in Table 1, and acronyms for the current branches are: The North Atlantic Current (NAC), the Rockall Trough Branch (RTB), the Sub-Arctic Front Branch (SAFB), and the Central Iceland Basin Branch (CIBB) (following [25])

nutrient concentrations. Key aspects of open ocean silicate limitation during summer and its influence on zooplankton and pelagic fish are also outlined in Sect. 2. Evidence for oceanic regulation of shelf ecosystems – across the shelf edge and tidal mixing fronts – is provided in Sect. 3. A summary is given in Sect. 4.




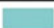









2 Nutrient Fronts in the Open Ocean

2.1 *The Main Thermocline: Currents and Water Masses*

Large parts of the World oceans are characterized by a layer of oxygen-poor, nutrient-rich intermediate water [33]. From a climatological spatial perspective, there is a general poleward shallowing of the isopycnals, bringing this biogeochemically distinct thermocline layer toward the surface in the north [34]. In the North Atlantic, the isopycnals steepen markedly between the major subtropical and subpolar gyres, establishing large-scale, persistent nutrient fronts near the surface – aligned with the North Atlantic Current (NAC) [35]. As the NAC – the boundary between the subtropical and subpolar gyre – passes east of the Mid-Atlantic Ridge, it encounters the Rockall-Hatton Plateau and subsequently the European Continental slope (Fig. 1). These topographical features split the NAC into three branches: (1) a branch that is deflected south toward the Bay of Biscay, (2) a branch that is channeled into the Rockall Trough, and (3) a branch that exists as a partial retroflexion into the Iceland Basin (IB) (Fig. 1a). The IB is surrounded by the Rockall-Hatton Plateau, south Iceland slope and the Reykjanes Ridge. In this region, the NAC further splits into the SAF branch that hugs the western slope of the Rockall-Hatton Plateau (Figs. 1a, b) and the Central Iceland Basin branch that veers west and marks the periphery of the SPG in the IB [25].

Numerous studies have presented zonal cross-sections between the European and the Greenland slope [20, 36]. Main characteristics are the relatively homogenous and saline Eastern North Atlantic Water mode water in the east (ENAW, Figs. 1b, e, Table 1), bounded by the stratified “floor” of the westward surfacing intermediate water (IW, Figs. 1c, e, Table 1) associated with the main thermocline. The IW is strongly influenced by the low-saline and nutrient-rich Subarctic Intermediate Water (SAIW, Figs. 1c, e, Table 1) that is formed near the surface in the central SPG/Labrador Current region and flows along isopycnals to greater depths while being transported eastward [35, 37] (Fig. 1c). The subtropical water carried eastward by the NAC, as it is influenced by the admixture SAIW, is referred to as Western North Atlantic Water (WNAW, [19, 38]), and this outlines the “south-eastern” periphery of the SPG (Fig. 1b, Table 1). The thermocline/IW layer envelopes the SPG and constitutes a major deep nutrient front in the NE Atlantic. The confluence and mixing of ENAW and WNAW produces Subpolar Mode Water (SPMW) – the dominant upper layer water mass in the study region [39] (Fig. 1b, e). The works by Brambilla and colleagues [25, 40] furthermore divided the SPMW into several density classes, separated horizontally by highly stratified water masses not

Table 1 List of water masses and their acronyms

| Water masses | | |
|--------------|---|---------------------------------|
| Acronym | Color | Name |
| AAIW |  | Antarctic Intermediate Water |
| ENAW |  | Eastern North Atlantic Water |
| IW |  | Intermediate Water |
| ISW |  | Iceland Slope Water |
| ISOW |  | Iceland-Scotland Overflow Water |
| LSW |  | Labrador Sea Water |
| MNAW |  | Modified North Atlantic Water |
| MOW |  | Mediterranean Overflow Water |
| NADW |  | North Atlantic Deep Water |
| SAIW |  | Subarctic Intermediate Water |
| SPMW |  | Subpolar Mode Water |
| WNAW |  | Western North Atlantic Water |
| AABW |  | Antarctic Bottom Water |

belonging to any SPMW class. These are carried polewards by the abovementioned intense current branches (Fig. 1a). Previous studies have treated the various SPMW classes as individual water masses (e.g., Modified North Atlantic Water, Iceland Slope Water, introduced later), and the popular term *Atlantic water* is a general reference to this water mass complex. Underlying these waters, and under the IW envelope, the low-salinity and relatively nutrient-rich Labrador Sea Water (LSW) comprises the main body of the SPG [41] (Figs. 1d, e).

South of the Rockall-Hatton complex, the IW is composed of oxygen-poor and silicate-rich Antarctic Intermediate Water (AAIW), transported northward under the Gulf Stream, and salty Mediterranean Overflow Water (MOW) ([42], Fig. 1c, Table 1). At larger depths east of the Mid-Atlantic Ridge, silicate-rich Antarctic Bottom Water (AABW) is also transported northwards extending into the Rockall Through and IB and onto the Rockall-Hatton Plateau (Fig. 1d, Table 1).

2.2 From the Thermocline to the Photic Zone

In order to contribute to the rich primary production in the NE Atlantic Ocean, nutrients must somehow be transported from and/or through the IW layer toward the photic zone. The gyre-scale circulation transfers fluid between the thermocline

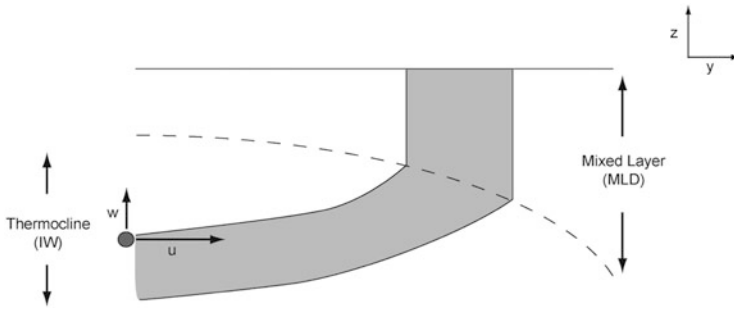


Fig. 2 A schematic figure of the Induction flux into the mixed layer. Fluid is being transferred from the stratified thermocline and into the mixed layer (gray region). A fluid particle is advected by the vertical velocity w and the lateral velocity u . (Redrawn from [33]; their Fig. 2.11a)

(IW layer) and the mixed layer/seasonal boundary layer [33]. This exchange is due to the time-mean circulation and consists of vertical and horizontal contributions:

$$\text{Exchange} = w_b + u_b \cdot \nabla \text{MLD} \quad (1)$$

where w_b and u_b are the vertical and horizontal velocity vectors at the base of the seasonal boundary, the depth of this layer is represented by the mixed layer depth (MLD), and ∇ is the lateral gradient operator (Fig. 2, from [33]). In the IB region, u_b is generally directed polewards, and the MLD also increases northwards ($\frac{\partial(\text{MLD})}{\partial y} > 0$) (see Fig. 6). This results in net transport into the seasonal boundary layer – a so-called *induction flux* [33], or *obduction* in the terminology of [40]. Over the subpolar gyre in general, fluid is transferred from the thermocline into the seasonal boundary layer by this *induction flux*. This process is essentially the reverse of the classical subduction process that produces the mode water on the warm side of the Gulf Stream [43]. The largely lateral induction flux in the SPG region totals 300 m yr^{-1} , compared to a vertical Ekman flux of only about 50 m yr^{-1} (where the volume fluxes are expressed per unit horizontal area, [33]). Hence, the surface waters around the periphery of the subpolar gyre are likely sustained through the horizontal and advective influx from the nutrient-rich thermocline/IW layer.

In contrast to the work of [33, 40] reported a net subduction in the northern NE Atlantic – not in the classical sense, but due to entrainment of thermocline waters into the overflows (Fig. 1d). The thermocline-to-boundary layer exchange estimates by these previous works were, however, solely based on air–sea interaction data and therefore lack details of the realistic flows and their interaction with the topography. If the near-thermocline flows are rectified by bathymetry (e.g., by the Rockall-Hatton Plateau), this could force the nutrient-rich IW into the seasonal boundary layer and thus strongly increase the induction flux (obduction) locally.

The region south of the Iceland-Faroe Ridge has previously been identified as a key water mass transformation area in the subpolar North Atlantic [44]. Through the

variable entrainment of SPMW/LSW/IW, northeastward extension of the SPG-limb is reported to regulate the properties of the Iceland-Scotland Overflow Water (ISOW, Fig. 1d) and thus the North Atlantic Deep Water downstream [45]. However, since the regional seasonal boundary layer can deepen to the depth range of the overflow and SPG water complex during winter (see Fig. 6), the energetic overflow has the potential to amplify an induction flux from the IW to the photic zone – an important process which has not received much attention in the literature.

By reviewing how the SPG shifts the frontal systems laterally in relations to the complex bathymetry in the NE (especially on and around the Rockall-Hatton Plateau), we discuss the induction fluxes and suggest locations for possible nutrient fertilizing “hotspots.”

2.3 *The Subpolar Gyre*

Linkages between the energetic atmospheric and oceanic dynamics and hydrography in the northeastern Atlantic are thoroughly discussed in the literature [19, 24]. The regional state of the atmosphere is typically represented by the North Atlantic Oscillation (NAO) index [46], while the state of the subpolar Atlantic marine climate has been proxied by the so-called gyre index [22, 24, 47] (Fig. 3) in addition to the Atlantic Multidecadal Oscillation (AMO) [49]. It is now well established that periods with a high NAO index (NAO+ states) are associated with a strong and expanded SPG [44], (SPG+ state, Fig. 1b, represented by a high gyre index, Fig. 3). This involves a northeastward expansion of the frontal complex and increased contribution of WNAW to the SPMW, at the expense of the ENAW. On the other hand, a weak NAO-/SPG- state is associated with generally southwestward frontal shifts (Fig. 1b) and an increased relative contribution of saline and nutrient-poor ENAW to the SPMW. The major salinification and warming of the NE Atlantic after the early 1990s was linked to an abrupt drop in the NAO index and a subsequent weakening and westward retraction of the SPG [24]. This is, admittedly, a simplification of this complex system. The relative importance of horizontal gyre changes and vertical mixing processes for influencing regional hydrography is still widely debated [40, 50].

Few studies have examined regional nutrient dynamics in the context of large-scale oceanographic features. Rey [51] linked a persistent decline in the upper ocean, pre-bloom (late winter) silicate concentrations along the Norwegian slope after the early 1990s to the weakening SPG. This was based on correlations between the silicate data and the gyre index. Similarly, in the Rockall Trough, Johnson et al. [38] linked a decline in the upper ocean nitrate and phosphate, but not silicate, to a weakening SPG and the associated dominance of nutrient-poor ENAW. More recently, Hátún et al. [52] revealed a steady silicate decline throughout a broad area of the subpolar Atlantic, including the Labrador Sea, Irminger Sea (Fig. 3), IB and the northern Nordic Seas since the early 1990s. In agreement with [51], this broad, pre-bloom silicate decline was primarily linked to the decline of the SPG,

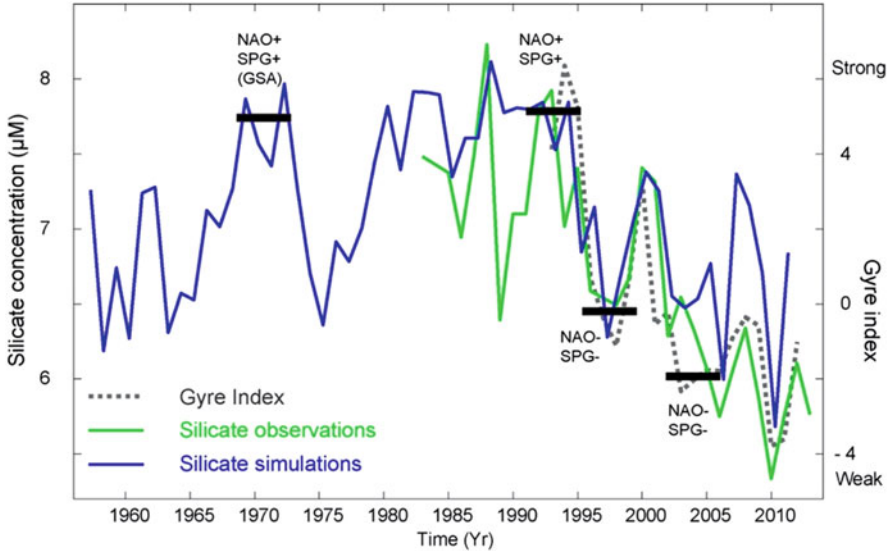


Fig. 3 Temporal evolution of silicate and the gyre index. The observed (green) and simulated (blue) pre-bloom upper ocean silicate concentrations (0–200 m, March) in the northern Irminger Sea (Ir in Fig. 4) are compared to the gyre index (dashed gray). The dimensionless gyre index is associated with the leading North Atlantic sea-surface height mode obtained from altimetry observations [48]. The samples have been taken in the pre-bloom homogeneous winter mixed layer several hundred meters thick. Periods with a strong/weak atmospheric forcing and subpolar gyre (NAO+/SPG+ and NAO-/SPG-, respectively) are emphasized. The 1970s Great Salinity Anomaly (GSA) period is also noted

with a possible contribution from a reduction in trans-Arctic silicate. In agreement with [38, 52] did not report any marked silicate decline in the Rockall Trough or south of this. By extrapolating station-based silicate records with a realistic ocean carbon cycle model HAMOCC [53], it is evident that the signal of silicate decline originates at the frontal zone at the southern tip of the Rockall-Hatton Plateau (Fig. 4).

The degree of silicate decline intensifies across the IB with especially strong imprints in the Reykjanes Ridge frontal region and along the IFF (Fig. 4). This spatial analysis indicates that oceanographic processes responsible for the observed silicate decline are likely to occur adjacent to and downstream of the IB. However, previous studies [38, 51, 52] did not attempt to quantify the relative importance of the vertical and horizontal SPG-related processes for explaining the silicate decline.

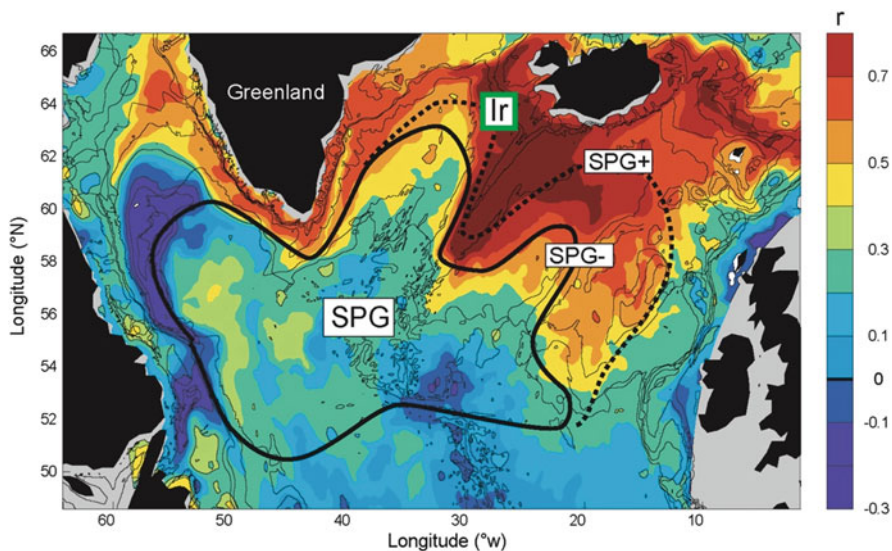


Fig. 4 Analysis of the simulated (HAMOCC) near-surface (0–150 m) silicate during March. The map shows the correlation between the simulated time series in the northern Irminger Sea (Ir, green box) and the time series at each individual model grid cell (1958–2011). The black lines outline the approximate boundary of the subpolar gyre during a weak state (SPG-, dashed) and a strong state (SPG+)

2.4 On and Around Rockall

2.4.1 South of Rockall

The SPG dynamics might impact the IW layer, even south of the Rockall Region. A long-term decrease in the oxygen concentration of the IW, with the largest changes occurring from 1993 to 2002 has been observed along a zonal repeat section at 48°N [54]. These changes were associated with the SPG contraction and thus reduced penetration of oxygen-rich IW of subpolar origin into the region. This allowed an increased northward transport of IW of subtropical origin, which is lower in oxygen. A decrease of preformed phosphate during the same period, especially in the density range of IW and MOW (along the 48°N section), supports the conclusion of a reduced influence from the SPG after the early 1990s ([54], see Fig. 3).

2.4.2 The Rockall Trough

The WNAW and ENAW meet in the Rockall Trough [19, 38] (Fig. 1b). In the deeper intermediate layer below, the confluence of contrasting SAIW/IW and MOW forms sharp lateral physical and biogeochemical gradients [55] (Fig. 1c, e). A strong,

eastward extended SPG increases the influx of SAIW into the Rockall Trough (Fig. 1b). It is thoroughly documented that such events lead to a marked freshening of the region and of the poleward flowing Atlantic water [24, 38, 56]. Strong SPG+ states and freshening periods – also referred to as Great Salinity Anomalies (GSAs, Fig. 3) [57, 58] – took place during the early 1970s and the early 1990s. Frequent sampling at the strategically located Ocean Weather Ship J at the southern tip of the Rockall-Hatton Plateau (52°30'N, 20°00'W, Fig. 1c) showed that SAIW comprised more than 35% of the 400–700 m water column during 1972–1975 [37]. This fractional contribution was suddenly reduced to below 5% during 1976 and remained very low during the rest of this record (was terminated in 1980). The influx of SPG-related subarctic water into the Rockall Trough increased by more than 2 Sv ($1 \text{ Sv} = 10^6 \text{ m}^3 \text{ s}^{-1}$) during the 1972–1975 and decreased again by the same amount from 1976 to 1980 ([24], their Fig. 4).

There has been a recent salinity decline in the NE Atlantic [59], which consisted of two marked drops – one between 2010 and 2012, and a very abrupt drop after 2015 (Fig. 5). Hydrographic data from the standard, repeat Extended Ellet Line section across the northern part of the Rockall Trough (Fig. 1c) revealed major salinity drops through the water column over the IW layer (0–1,000 m) along the eastern side of the Rockall-Hatton Plateau during both events (Figs. 5c, d). After remaining within the ENAW salinity range (>35.30) for about two decades (~1996–2016), the salinity in this region dropped below 35.2 during 2016. This is a clear indication of increased presence of SAIW. Both the salinity values and the temporal trend in the Rockall Trough Branch are very similar to the properties in the Atlantic water inflow to the Nordic Seas observed in the Faroe Bank Channel (Fig. 5b). There has also been a marked salinity decrease in the SAF Branch in the IB since the early 2000s (Figs. 1a and 5b). However the salinity of this flow is much lower than the salinity observed in the Faroe Bank Channel, and the 2010–2012 and 2015–2016 drops are less evident.

This all indicates that the Rockall Trough Branch is a more direct source to the waters west of the Faroe Plateau than is the SAF Branch. In the same way that the increased influx of low-salinity SAIW leads to freshening events, this nutrient-rich water mass also leads to increased nutrient concentrations – especially along the western side of the Rockall Trough entrance [56]. The major salinity drop around 2015–2016 was accompanied by a marked silicate increase of about $1 \mu\text{M}$ off the Faroe shelf, in the northern IB and in the northern Irminger Sea (see Fig. 15 herein, adapted from [60]). This disrupted the persistent silicate decline that has characterized the entire subpolar Atlantic since the early 1990s [52] (Fig. 3).

In summary, (1) a strong SPG shifts the SAF from the IB to east of the Rockall-Hatton Plateau (Fig. 1b), which leads to strong near-pycnocline flows into the deep seasonal boundary layer of the Rockall Trough, and (2) this intensified and topographically rectified Rockall Trough Branch will markedly increase the induction flux of nutrient-rich subarctic water to the Atlantic inflow waters. We propose this area (referred to as Region 1 in Fig. 6b) as a key *fertilization hotspot*.

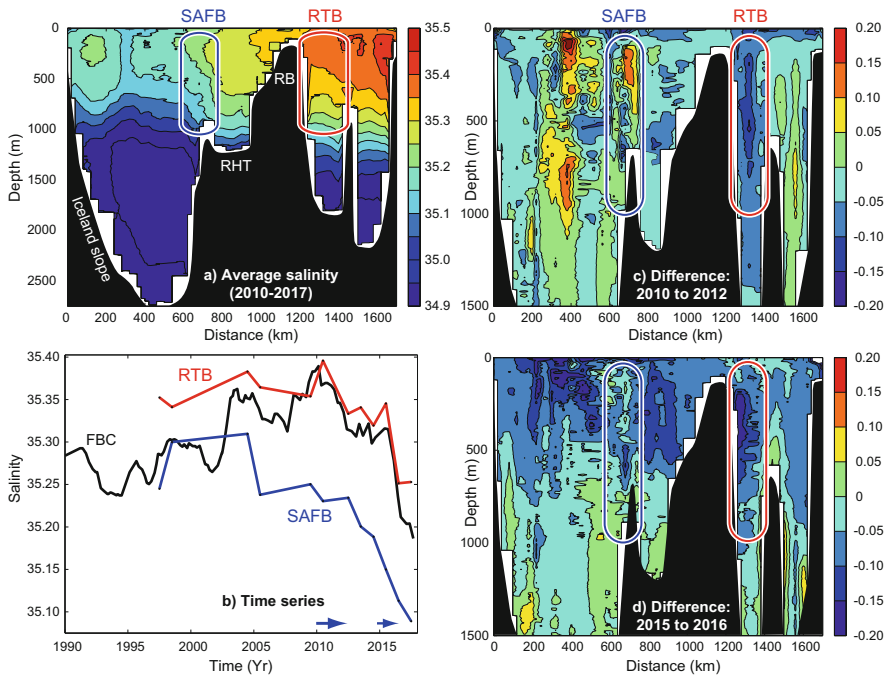


Fig. 5 Salinity along the Extended Ellet Line (EEL, Fig. 1a). (a) Average over the period 2010–2017 based on yearly CTD sections (no section available for 2011). (b) Time series, based on averages across the Sub-Arctic Front Branch (SAFB), the Rockall Trough Branch (RTB) – blue and red rectangles – and the salinity in the upper Atlantic water layer in the downstream Faroe Bank Channel (FBC, black). Sectional views of the salinity difference over the two major declining steps evident in the RTB and FBC series (blue arrows in b) are shown in (c) 2010-to-2012 and (d) 2015-to-2016. Bathymetric abbreviations: Rockall-Hatton Trough (RHT) and Rockall Bank (RB)

2.4.3 On the Rockall-Hatton Plateau

A near-bottom flow below the oxygen minima brings silicate-rich water ($\text{Si} > 15 \mu\text{M}$), enriched by Antarctic Bottom Water (AABW), northwards through the Rockall-Hatton Trough, which is located between the Rockall and Hatton Banks (Fig. 1d, Table 1) [42]. A modeling study [23] identified especially large inter-annual variability in winter MLDs in the very same region (Region 2 in Fig. 6b), which likely is enhanced by topographic effects of the Rockall-Hatton Plateau. Intensified surface heat losses and wind stress curls prior to 1995 (NAO+ state, Fig. 3) resulted in deep MLDs, with a potential to induce large upwelling of silicate. The resulting vertically homogenous mode water advects northward between the Faroese banks and joins the SPMW complex south of the Iceland-Faroe Ridge. The SPMW complex is a reservoir for the Atlantic water flowing westward toward Greenland and northeastward between Iceland and the Faroe Islands, also referred to as Modified North Atlantic Water (MNAW, Fig. 1b, Table 1) [61]. After 1995, the atmospheric forcing weakened considerably and the MLDs on the Rockall-Hatton Plateau became

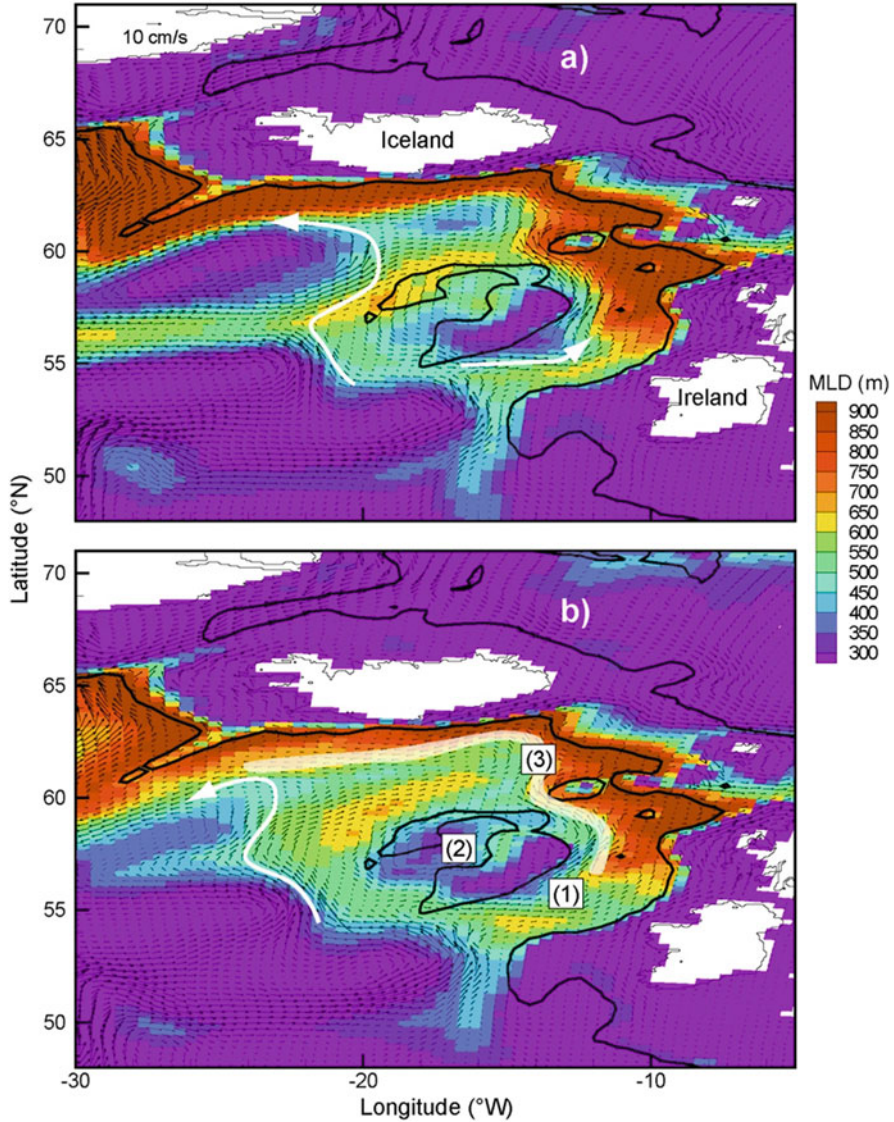


Fig. 6 Simulated mixed layer depths (colors) and velocities (small arrows) in March during (a) an intense NAO+/SPG+ period (1990–1995) and (b) a more relaxed NAO-/SPG- period (1996–2001). The figure is adapted from the study by [23], which was based on the Miami Isopycnal Ocean Model (MICOM) – the same model system as used by [24] to calculate the first gyre index. The black contour line corresponds to 1,000 m depth. Potential fertilization hotspots locations are shown with the numbers in (b), where the gray band outlines hotspot (3). Large white arrows emphasize flow anomalies in the Rockall Trough Branch (a), and in the Central Iceland Basin Branch (a, b) (see Fig. 1a), respectively

gradually shallower (NAO- state, Figs. 3 and 6b). The re-intensified atmospheric forcing (NAO+/SPG+) state after 2014 resulted in a marked densification of the seasonal boundary layer and deeper MLDs again in this region (see Fig. 8, below). Although the linkage to frontal dynamics is less direct here, we propose the Rockall-Hatton Trough (Region 2, Fig. 6b) as the *second nutrient fertilization hot spot*.

2.5 The Iceland Basin

When integrated across the Ellett Line in the northern Rockall Trough (Fig. 1a), the SPG-related fertilization is evident in nitrate and phosphate but not in silicate [38]. However, an analysis of individual oceanographic stations has revealed a negative trend (1990 to present), which becomes increasingly evident as one moves west from the European Continental Slope across the Rockall-Hatton Plateau into the central IB and toward the south Iceland slope ([52], their Fig. S1). These data support our previous conclusion that the mechanism behind the silicate decline is likely to be found in the vicinity of the IB, as demonstrated with the model result in Fig. 4.

The boundary between the relatively well-stratified SPG water masses and the deep seasonal boundary layers manifests itself as a band of steep isopycnals all the way from the northern Rockall Trough to the eastern flank of the Reykjanes Ridge (Fig. 6). According to Eq. (1), the strong flows in this region (large u_b) and the steep isopycnals (large ∇ MLD) establish a potential for large induction fluxes through this broad, deep front.

The real flows are more complex than those outlined by [25] (Fig. 1a). Inter-annual variability in the currents' strength and position is pronounced (Fig. 6) [24]. The SAF-associated current branches east and west of the Rockall-Hatton Plateau are locked to the topography (Figs. 1a, b and 6), and the relative strength of these branches varies in relation to the strength and size of the SPG. So horizontal frontal shifts in this region are "discretized" in a similar manner as the NAC is channeled through the fracture zones farther west along the Mid-Atlantic Ridge [55]. The SAF Branch in the IB is always present, but it remains uncertain whether it continues directly through the Iceland-Faroe gap [25, 62], or if the Rockall Trough Branch folds west on it, and a confluenced flow veers westward in the northern IB (Fig. 6). The results in Fig. 5 (Sect. 2.4.2) indicate that the SAF Branch cannot be the sole source for the water west of the Faroe Islands, while the Rockall Trough Branch is a more viable, direct candidate.

The location and strength of the Central Iceland Basin Branch is shifting continuously along a northeast-southwest axis, intimately related to the SPG dynamics (see below). The schematic representation from [21] of a cross-section downstream of the Faroe Bank Channel overflow plume (here extend southwestward to the central IB, Fig. 7) gives a vertical perspective of the frontal shifts in the IB, and associated impacts on the induction fluxes and water mass composition. The SPG-limb in the IB consists of an oxygen-poor (Figs. 7 and 8), nutrient-rich IW layer over a thicker

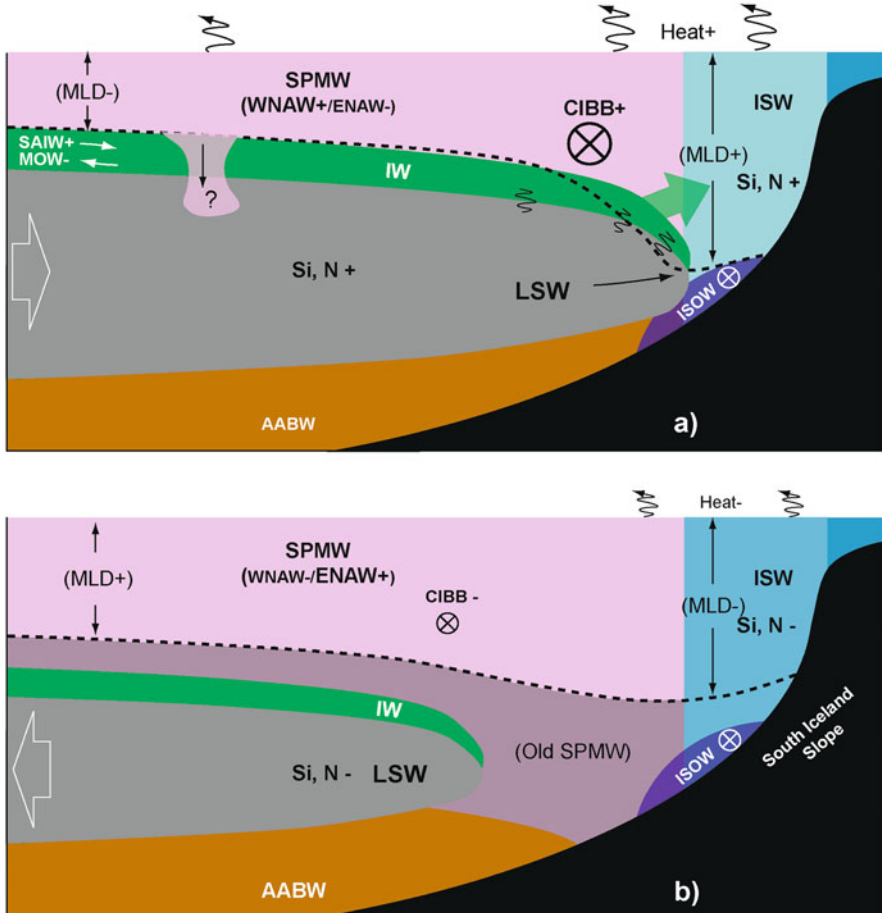


Fig. 7 A schematic representation of a cross-section downstream of the Faroe Bank Channel overflow plume. It extends from the central Iceland Basin (left) to the South Iceland slope (right) (see Fig. 1c) during a (a) NAO+/SPG+ state and (b) NAO-/SPG- state. Abbreviations: Silicate (Si), nitrate (N), the Central Iceland Basin Branch (CIBB), and the mixed layer depth (MLD). The black dashed line illustrates the depth of this mixed layer. Water masses are color coded in correspondence to Fig. 1, and Table 1, and the water mass acronyms are provided in this table. Inspired by [21] (their Fig. 13). Note that the details around whether or not vertical winter mixing interacts with the LSW are tentative

body of LSW. The IW layer continues north through the IB, where it has a doming structure over the central basin, in addition to its general westward shoaling toward the Reykjanes Ridge [63] (Figs. 1e and 8a). It terminates at about 2000 m depth along the south Iceland slope (at 20°W, [64]), but might reach as far northeast as the Faroe Bank Channel overflow plume [21, 65] (Fig. 1c).

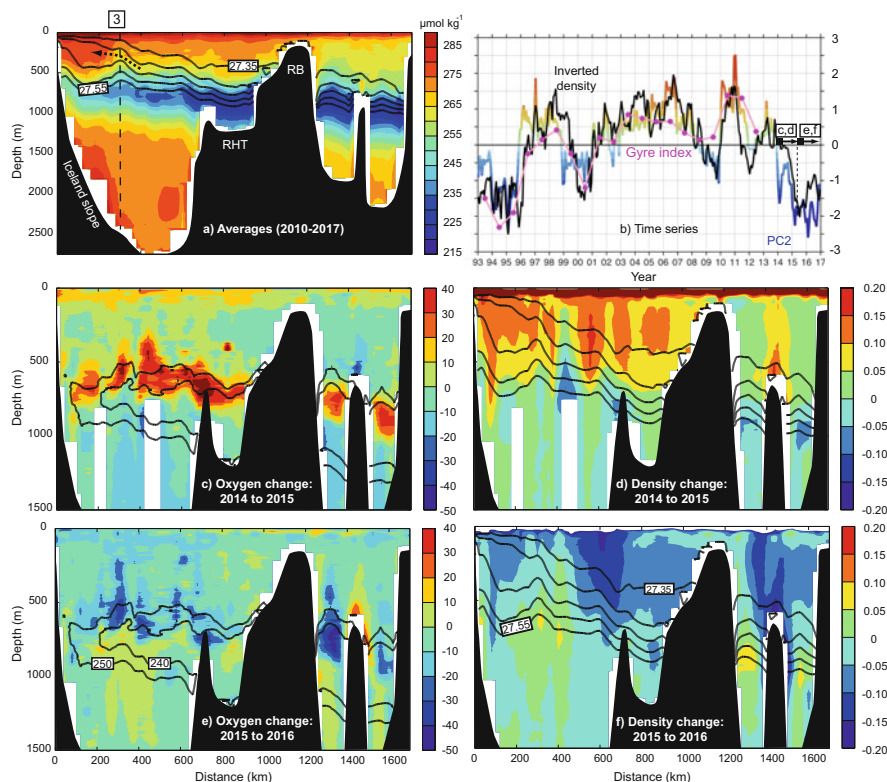


Fig. 8 Oxygen and potential density (σ) along the Extended Ellet Line (EEL, Fig. 1c). **(a)** Averages over the period 2010–2017 showing oxygen with colors and σ with black contours, based on yearly CTD sections (no section available for 2011). **(b)** Time series of the gyre index (pink), the density over the Iceland Basin, Reykjanes Ridge and Irminger Sea region (black) and the second principal component (PC2) from an updated analysis of the re-worked satellite altimetry data (colored, from [22]). The oxygen changes from 2014 to 2015 (the strongest recent convection event, see **b**) and from 2015 to 2016 (weaker atmospheric forcing) are shown in panels **(c)** and **(e)**, respectively. The averaged oxygen from panel **(a)** is, in **(c)** and **(d)**, contoured at 240 and 250 $\mu\text{mol kg}^{-1}$, for comparison (black lines). The corresponding changes in σ are shown in **(d)** and **(f)**, respectively. The black dashed arrow in **(a)** illustrates the potentially large induction flux; the suggested nutrient fertilization Region 3 (see Fig. 6) is highlighted. Bathymetric abbreviations: Rockall-Hatton Trough (RHT) and Rockall Bank (RB)

Over the SPG-limb, we have a slab of SPMW. The slope-hugging, oxygen-rich ISOW (Figs. 1d, 7 and 8a, Table 1) plume underlies the Iceland Slope Water (introduced below) near Iceland.

SPG dynamics strongly regulate the water mass contribution into the IW layer in the IB [63]. A strong gyre leads to more nutrient-rich SAIW and less MOW [56, 66] (Figs. 1c and 7) and thus higher nutrient concentrations in the IW. Whether or not the gyre influences the AAIW contribution to the IW is an open question. The silicate concentration in the LSW also increases with an intensified SPG through the

associated deeper convection in the Labrador-Irminger Seas [52]. This signal should reach the IB (Fig. 7) after a 1–2 years advective lag [67].

2.5.1 The Central Iceland Basin Branch

Northward expansions of the SPG-limb and an associated northward shift of the Central Iceland Basin Branch in the IB during NAO+/SPG+ states (Figs. 1b, 6a and 7a) are caused by the combined impact of increased volumes of LSW and intensified Ekman pumping [33]. According to model simulations ([23], Fig. 6), the main IW-layer rises in the central IB during NAO+ states, resulting in reduced winter MLDs there (Figs. 6a and 7a). In contrast, winter MLDs deepen in the Rockall-Hatton Trough and along the south Iceland slope and the eastern side of the Reykjanes Ridge (Fig. 6). This results in markedly increased pycnocline gradients (∇ MLD) around the central IB (Figs. 6a and 7a). At the same time, both the meridional SAF Branch west of the Rockall-Hatton Plateau and the Central Iceland Basin Branch strengthen (stronger u_b). The increased ∇ MLD, u_b , in addition to the increased volume of – and nutrient concentrations in – the SPG-limb water, all likely contribute to stronger induction fluxes of nutrients to the northern IB. We propose that the front associated with the steep isopycnals along the northern rim of the SPG in the IB is a broad nutrient fertilization region (Region 3, Figs. 6b and 8a).

2.5.2 Interaction with the Overflows

The SPG-limb in the IB can bring IW/LSW all the way north to the slopes of the Iceland Plateau and the Iceland-Faroe Ridge [21, 65]. Here IW/LSW can interact directly with SPMW above and ISOW below (Figs. 1 and 7a). While the importance of entrainment, or subduction, of lighter water masses into the overflows has been thoroughly discussed in the literature [21, 44], the possibility that overflows could also induce induction fluxes, or obduction, has not received much attention.

The secondary transverse circulation around the overflow plume from the Faroe Bank Channel transports ISOW “downhill” in a thin Ekman layer and draws the nutrient-rich/oxygen-poor IW northwards over the plume [68] (Figs. 1c and 7). The energetic overflow plume induces mixing, most strongly near the seafloor, but also in the ambient overlying waters due to e.g. breaking internal waves [68]. Increased activity of topographic Rossby waves are also observed along the southern slope of the Iceland-Faroe Ridge, all the way from the Faroe Bank Channel plume to the Icelandic continental rise [69, 70]. Seaglider data furthermore reveal that vertical dissipation is elevated along the Iceland-Faroe Ridge, although much intensified near the overflow plume and in the fast deep flows along steep topography near Iceland [71]. Bottom-up mixing effects of topography and the overflow plume likely invigorate regional winter convection. This could thus partly account for the very deep seasonal boundary layer along the Faroe-Bank Channel-to-Reykjanes Ridge swath, slope-ward of the fertilization band marked (3) in Figs. 6b and 8a.

Mixing along the Iceland-Faroe Ridge produces the Iceland Slope Water (ISW), residing within the 2000 m isobaths south of Iceland and along the eastern side of the Reykjanes Ridge (Figs. 1c and 7). It has previously been suggested that the ISW is a mixture primarily of SPMW and ISOW, with some additional LSW in varying mixing ratios [64]. Recent studies near the overflow plume, however, suggest that the IW will contribute to the ISW as well [21]. We therefore find it likely that the overflow plume amplifies the induction flux of nutrient-rich LSW and IW to the SPMW and ISW (Region 3, Figs. 6 and 8).

This effect is probably stronger during SPG+ states, when the northeastward extended SPG-limb in the IB brings the subarctic waters closer to the topography/overflow “blender” [21]. On the other hand, the transport of ISOW becomes weaker during years with strong wind stress curl (NAO+/SPG+ state) over the Nordic Seas, which concurs with an SPG+ state [72–74]. At present, we can only speculate whether this potentially weaker “blender” will have any appreciable effect on the mixing efficiency along the south Iceland-Faroe Ridge slope.

2.5.3 Potential Convection into the IW Layer

An important remaining question is to what degree winter convection reaches into the thermocline in the central IB. According to simulations, the rise of the thermocline during NAO+/SPG+ states reduces the winter MLDs in the central IB (Fig. 6), which gives an impression of reduced vertical mixing of deep water. However, this also brings the nutrient-rich IW-layer closer to the convection zone, which together with the intense surface heat losses could increase the upwelling of nutrients from the IW-layer.

Johnson et al. [75] reported much higher oxygen concentrations in the IW during the strong NAO+/SPG+ state in 1993 compared to the weak NAO-/SPG- state in 2003 (see Fig. 3). They interpreted this as evidence for a stronger ventilation of the IW during 1993. The strong atmospheric forcing during the winter 2014–2015 resulted in revived deep convection in the Labrador-Irminger Sea [76, 77] and generally denser seawater in the Irminger Sea, Reykjanes Ridge and IB region – that is an intensified SPG (Fig. 8b, from [22]). New data from the Extended Ellet Line reveal a marked densification throughout the upper layer waters during 2015 (Fig. 8d), and a major positive oxygen anomaly is evident along the top of the IW-layer (500–800 m depths, Fig. 8c) – an indication of deeper convection and ventilation of the IW-layer. This is in agreement with [75]. The subsequent winter (2015–2016), with again weaker atmospheric forcing, resulted in a negative upper layer density anomaly (Fig. 8f) and a negative oxygen anomaly in the upper part of the IW-layer (Fig. 8e).

The strong oxygen-nutrient correlation in the IB [42] implies that vigorous ventilation events like in 1993 and 2015 would also increase the flux of nutrient-rich IW toward the surface. So vertical contribution to the induction flux (w_b) can potentially be substantial in the central IB during years with strong air-sea forcing. That is, the gray region in the seasonal boundary layer in Fig. 2 would be broad,

higher in the water column, and the nutrient fertilization would be more efficient throughout the IB.

Despite the identifiable impact of convection in the Rockall Trough, recent studies conclude that frontal shifts and its impact on lateral advection are much more important for the water mass properties in the Rockall Trough than vertical convection [78].

2.6 *An Integrated Perspective: In the Context of Sea-Surface Height, MLD, and the Gyre Index*

Sea-surface height (SSH) variability over the open ocean subpolar Atlantic is primarily determined by steric effects – that is changes in the integrated density over the entire water column [79, 80]. We discuss here the proposed induction flux hotspots against the backdrop of the simulated winter MLD and SSH fields in the North Atlantic combined with satellite altimetry.

In regions with strong winter convection, surface heat losses intensely cool the entire seasonal boundary layer, and this densification determines the depth of the boundary layer (Fig. 8). In such *convective domains*, a winter with strong heat losses (NAO+ state) results in both large MLDs and depressed SSHs induced by the steric contraction of the anomalously deep and dense boundary layer. That is, correlations between the MLD (positive with increasing depth) and SSH are negative in a *convective domain*.

There are also regions where the depth of the permanent thermo/pycnocline is determined by other processes than convection, e.g. Ekman pumping or lateral pressure gradients in the deep sub-thermocline layer. In such *advective domains*, a rise of the thermocline fills a larger part of the water column with cold and dense deep water, and the SSH drops – again due to steric contraction. That is, correlations between MLD and SSH are positive in an *advective domain*.

Utilizing the model system presented in [81] – the Max Planck Institute Ocean Model (MPIOM) – we identify the following areas as *convective domains* (negative SSH-MLD correlations, blue in Fig. 9): most of the Labrador Sea, the entire Irminger Sea, the Reykjanes Ridge, and the near-slope zone all around the NE Atlantic. In contrast, the central IB and waters south of the Rockall-Hatton Plateau and into the Rockall Trough entrance clearly outline an *advective domain* (positive SSH-MLD correlations, reddish in Fig. 9). As a digression, the biologically productive frontal zone in the NE Labrador Sea [82], associated with the strong west Greenland Current and the shedding of large Irminger Rings (eddies) [83], is also an advection-dominated region (Fig. 9).

During an intense winter (NAO+ state), the SSH is depressed throughout the subpolar North Atlantic, and the MLD in the convective domains deepens (blue in Fig. 9). The western mode waters (mostly LSW, [81]), produced in the Labrador and Irminger Seas, slide eastwards in and under the main thermocline in the advective

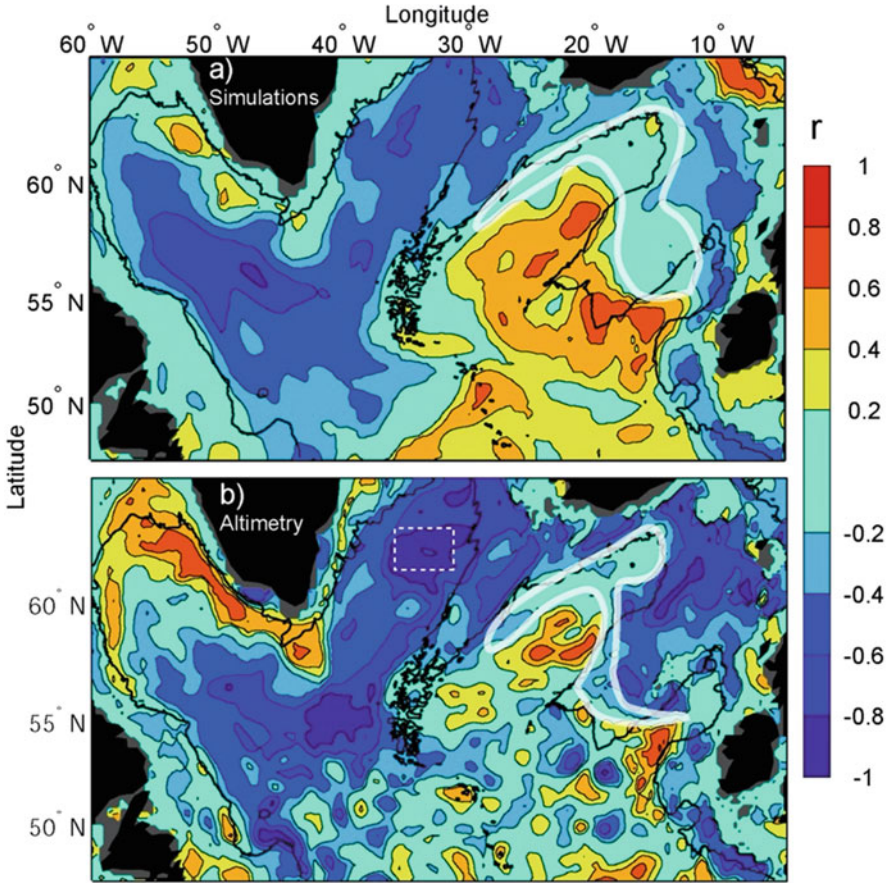


Fig. 9 Convective and advective domains. Correlation coefficients (r) between simulated March MLD and annually averaged (a) simulated SSH and (b) satellite altimetry. The simulations are obtained from the MPIOM model system presented in [81]. Negative values (blue) show *convective domains*, where deep winter mixing regulates the SSH, and positive values show *advective domains* (reddish), where the SSH variability is mainly determined by remotely forced undulations of the permanent thermo/pycnocline. The boundary between these regions in the NE, where large lateral induction fluxes are expected, is emphasized with the thick white curve. The 2000 m isobath is shown for reference, and the white dashed rectangle shows the region represented by the MLD time series in Fig. 10

domain. This, in turn, lifts the IW-layer in the central IB and Rockall Trough region and the winter MLDs there become shallower. That is, the eastern SPG-limb becomes inflated, and the gyre expands eastwards – partly driven by the curl of the wind stress field (e.g., [36]). During such NAO+/SPG+ states, the boundary between the convective and advective domains in the NE Atlantic (Fig. 9) must be characterized by steep isopycnals (large ∇ MLD) and thus high induction fluxes (Eq. 1). The high induction flux frontal zone from the Rockall Trough, crossing the

Rockall-Hatton Plateau and roughly following the 2000 m isobaths around the IB (Fig. 9) roughly coincides with the previously proposed nutrient fertilization hotspots.

The gyre index, which is calculated from the SSH field over the North Atlantic [24], is intrinsically linked to the above-discussed morphology of the seasonal boundary layer (Fig. 9). The temporal development of these processes since 1950 is summarized in Fig. 10, using the model-based gyre index [24], the altimetry-based gyre index [48], and the simulated SSH and MLD in the northern Irminger Sea, previously presented by [81].

2.7 After Established Summer Stratification

As soon as air-sea heat exchanges during spring/early summer become positive into the ocean, a relatively shallow mixed layer forms (~50 m). Around this period – potentially advance or delayed by other eddies and other turbulence inducing processes [10] – the spring bloom is initiated [8]. The silicate content in the summer mixed layer within the central IB is exhausted by the fast-growing diatoms within a week or two after the onset of a major bloom [12]. In the absence of an upwelling agent after bloom initiation, the growth of diatoms terminates and these relatively large and heavy algae quickly subside in a major export event out of the photic zone [84]. In the southeastern part of the IB, silicate depletion ($<2 \mu\text{M}$) takes place already in early May, earlier than in the Irminger Sea where it typically occurs in July–August [12]. In general, the Irminger Sea is a biologically much more productive region compared to the IB [85]. At first, this appears as a conundrum, considering that the IB region appears to determine pre-bloom upper ocean Si concentrations in the Atlantic inflow toward the Arctic and the Labrador Sea [52]. Although the altimetry-derived eddy kinetic energy – which expectedly should enhance vertical mixing – is very high in the IB [86], eddy slumping and/or wind-driven Ekman transports might only initiate stratification and blooms in the IB a bit earlier than expected from explicit consideration of air-sea heat exchanges [9]. The turbulent mixing of nutrients up through the seasonal thermocline is still lower in the central IB (*advective domain*, Fig. 9) compared to the adjacent Irminger Sea (*convective domain*) [85]. Consequently, the IB becomes biologically poor during summer, with low nutrient, phytoplankton/chlorophyll, zooplankton, and fish abundances/concentrations [85, 87]. According to logbooks, little fishery activity has historically taken place in the central IB (G. J. Óskarsson, pers. comm.) and pelagic fish surveys (redfish, mackerel, blue whiting, and herring) all end at the border of the IB [88].

2.7.1 A Bottom-Up Mackerel Case Study

In order to illustrate potential impacts of nutrient limitation on higher pelagic trophic levels, we summarize a recent study involving phytoplankton, zooplankton, and

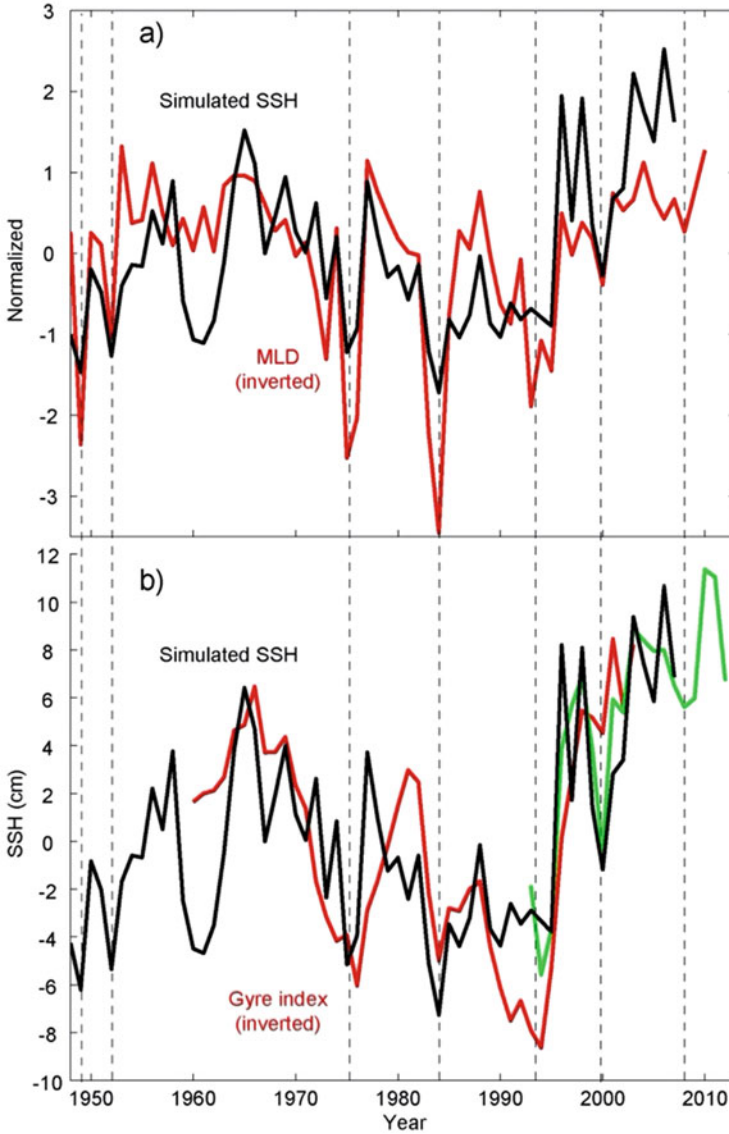


Fig. 10 Temporal development of key metrics for the thickness of the seasonal boundary layer (Fig. 9). (a) Simulated SSH (black) and MLD anomalies (red, inverted) within the Northern Irminger Sea box (white dashed rectangle in Fig. 9), normalized by the standard deviation. (b) The same simulated SSH time series (black) compared to two previously published gyre indices (inverted), based on satellite altimetry (green) [48] and simulations (red) [24]. The vertical dashed lines emphasize NAO+/SPG+ states, with strong air-sea forcing, deeper winter convection and an intensified SPG circulation

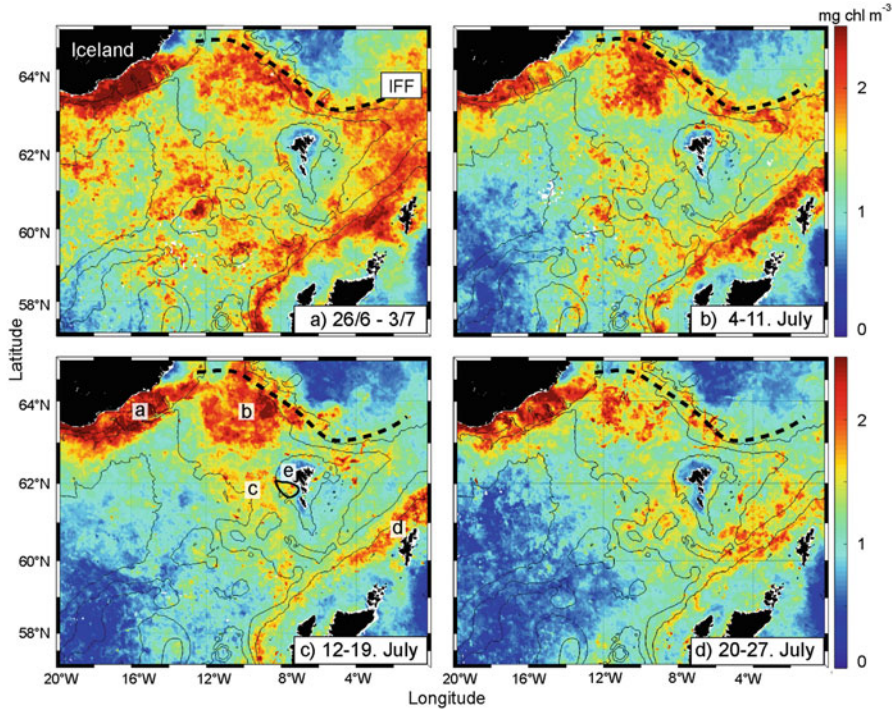


Fig. 11 Average near-surface chlorophyll distribution (mg Chla m^{-3}). Climatological averages (1998–2015) over four eight-day time segments from late June to late July (specific dates are shown in the part labels) are shown (from [17]). The dashed black line outlines the Iceland-Faroe Front (IFF). The letters in panel c) refer to the regions mentioned in the text (Sect. 2.7.1). These gridded satellite data were downloaded from the GlobColour Project, ACRI-ST (<http://www.globcolour.info>). Eight-day temporal averages of Level 3, merged (SeaWiFS, MODIS, MERIS, VIIRS), GSM-gridded [89] chlorophyll (CHL1) data were used on a 4-km horizontal grid for the period 1998–2015

Atlantic mackerel (*Scomber scombrus*) [17]. After having spawned along the European continental slope near Ireland during spring, starved mackerel are in critical need of food. Very low abundance of their preferred food item – the copepod *C. finmarchicus* [90] – in the spawning region forces mackerel to migrate north to more productive waters.

Accumulation of phytoplankton, and therefore likely of calanoid copepods (mackerel food), is confined to the near-topography or near-front regions upwelling hotspots through the summer (Fig. 11). Through July, the IB becomes virtually devoid of surface chlorophyll, while elevated concentrations persist in the following regions: (a) on and immediately off the south Iceland shelf, (b) shallow parts of the Iceland-Faroe Ridge and along the IFF, (c) the continuously mixing Faroe Bank Channel plume, (d) along the European Continental slope frontal zone, and (e) in a

small indentation on the western side of the Faroe shelf (Western Region, see Sect. 3.2.1).

Nutrient limitation has particularly strong impact on mackerel migration along the northern rim of the IB, where the mackerel is not near any thermal threshold. Data from a meridional repeat section along 20°W (Extended Ellet Line and WOCE A20, Fig. 1c) shows that the upper 50 m in the central IB becomes Si-exhausted in June, while there is a “corridor” near the south Iceland shelf with persistently non-limiting Si concentrations (Fig. 12, north of 63°N). Furthermore, data from international mackerel surveys during July show that both the zooplankton and the mackerel abundance are very low in the central IB. The biomasses are much higher in the “corridor” in Fig. 12 during both SPG+ and SPG- states. This “corridor” overlaps with the frontal zone along the ISW band (Fig. 1b) and the shelf [17], and the increased biological production is likely associated with topographic/overflow plume mixing processes and lateral induction fluxes from the rim of the SPG.

2.7.2 Gyre Impact on the Summer Conditions

NAO+/SPG+ states will set higher pre-bloom nutrient concentrations in the seasonal mixed layer and thus increase the new production. However, if not replenished by eddy stirring or summer storms, the initial mixed layer nutrient content is quickly exhausted [84]. Elevated winter concentrations may therefore only have a moderate impact on higher trophic levels, which are in continuous demand of food throughout the summer. However, in locations that experience recurrent mixing events throughout the summer, such as frontal zones, biological production can be sustained. The dynamics associated with the SPG can contribute to this process by increasing nutrient inventories in the sub-surface waters near frontal and topographic upwelling regions, and thus the replenishment of surface nutrient stocks in these production hotspots. In the case of mackerel, the Norwegian Sea and especially the IFF region have historically been the preferred feeding areas. A marked shift occurred around 2006, when mackerel started to expand west toward Greenlandic waters. Pacariz et al. [17] discussed this major mackerel expansion in the context of the SPG-related nutrient decline (Fig. 3), and the strong zonal Si gradient with climatologically low concentrations west of the British Isles, and high concentrations in the Irminger Sea.

Although the NAO primarily documents variability in winter weather conditions, there are also indications that NAO positive periods are associated with a higher frequency of summer storms [91]. This could drive enhanced vertical mixing events and, through associated nutrient replenishment, increase new production in summer months in the central IB. In contrast, [92] find that the establishment of a summer mixed layer is probably independent of the preceding winter conditions. Understanding the possible impacts of NAO variability on summer nutrient replenishment therefore warrants future research.

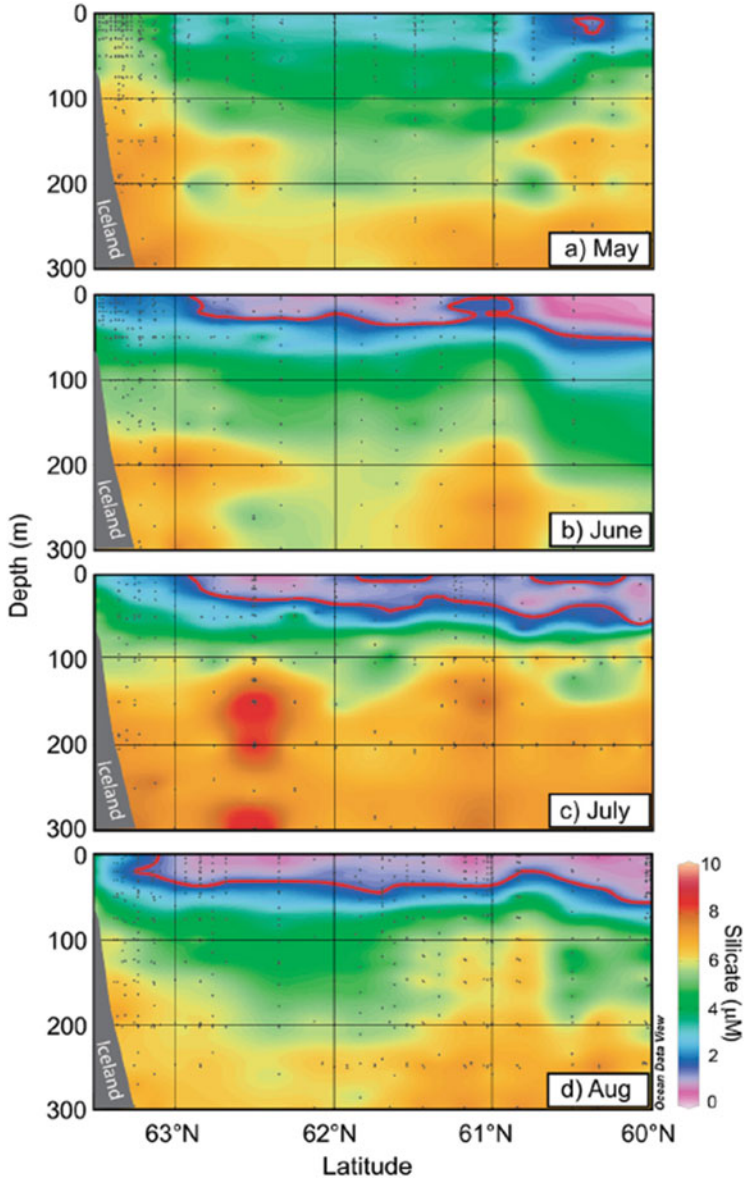


Fig. 12 Climatological silicate concentrations (μM) along the meridional WOCE/EEL section at 20°W (Fig. 1c) in (a) May, (b) June, (c) July, and (d) August. The red contour line emphasizes the limiting silicate concentration of $1.5 \mu\text{M}$ (from [17])

3 Onwelling to Adjacent Shelves

Broad-scale nutrient dynamics in the NE Atlantic likely exert a major impact on adjacent shelf ecosystems (i.e., the Northwestern European slope (NWES), North Sea, Faroe shelf, and the south Iceland shelf). In this section, we review recent literature on NE Atlantic-to-North Sea linkages. These considerations are based primarily on model simulations, but also aim to take into account emerging observations of shelf ecosystems. The Faroe Shelf area is described in detail since observations from this system, which is spatially confined and thus “surveyable,” could provide a useful framework for enhancing our general understanding of ocean–shelf interactions.

3.1 *From the Northeast Atlantic to the North Sea*

There is now a broad consensus that nutrient budgets in the open shelf areas of the NWES, and in the deeper parts of the North Sea, are dominated by nutrient fluxes from the NE Atlantic [27–29, 31, 93–97] – also referred to as “nutrient onwelling” [31]. Nutrient fluxes depend both on water mass exchange rates and nutrient gradients between the open ocean and the shelf seas. Some previous studies have reported increased nutrient fluxes during NAO+ phases, when intensified winds likely increase the transport of oceanic water onto the shelf [29, 96]. Recent studies, on the other hand, conclude that it is the open ocean nutrient concentration, more so than the influx volume, that primarily controls nutrient onwelling to the North Sea [27, 31, 94, 95]. Many of the initial NE Atlantic-North Sea studies, however, considered climate change scenarios, based on model simulations.

3.1.1 Future Projections

A general shallowing of the winter MLD during the twenty-first century, caused by increasing air temperature and accompanying weakened air-sea heat fluxes, is a robust feature in most climate models used in the Intergovernmental Panel on Climate Change (IPCC) reports [98]. These climate models project a particularly strong decline in the NE Atlantic MLD and pre-bloom nutrient inventories, which in turn could lead to a marked reduction in primary production within the present century [95]. The simulated MLD projections rely primarily on one-dimensional (vertical) mixing schemes and are thus heavily influenced by reduced heat losses from the oceans to the atmosphere [27]. It has been acknowledged that large-scale circulation changes may also play a role, but up until recently only vague statements about shifting currents have been made [95].

Recent studies have identified the importance of variable horizontal gyre circulation and its potential to regulate water mass balance in the NE Atlantic (Sect. 2) –

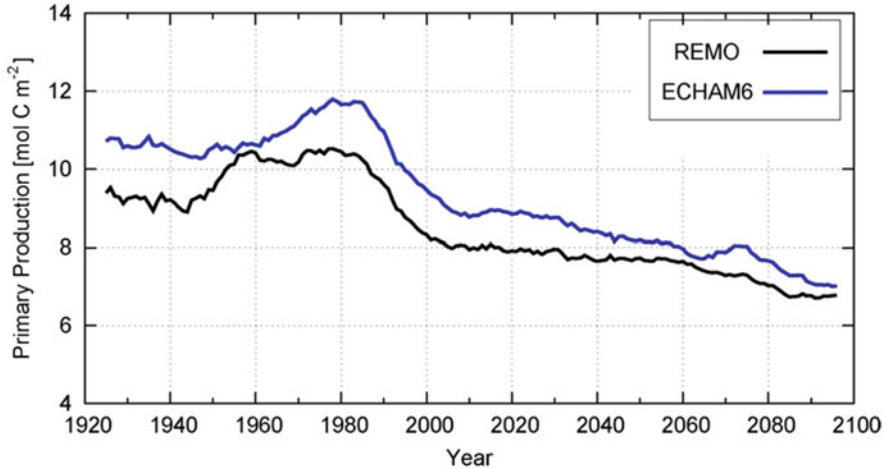


Fig. 13 Time series of annual accumulated depth-integrated primary production in the North Sea (10-year running mean, simplified from [27]). Shown are outputs from the regional climate model REMO and from the general circulation model, ECHAM, developed by the Max Planck Institute for Meteorology

and subsequently to the North Sea [27]. Global models have large deficiencies in the SPG domain, and elaborate bias corrections are required to introduce realistic hydrographic gradients, such as encountered in frontal zones [27]. The predicted nutrient decline in the SPG and in the NE Atlantic [98] is especially evident in regionalized models that are characterized by a higher spatial resolution. The first study to explicitly discuss the potential connections between the SPG and the North Sea was based on a global version of HAMOCC [27]. The same model system was used by [52] to contextualize the observed silicate decline in the subpolar North Atlantic both in time and space (Figs. 3 and 4). The projection run by [27] shows a reduction in primary production throughout the twenty-first century, although at slower rates than during the 1980–2000 period (Fig. 13).

The projected properties in the North Sea are inherited from the open ocean, but climate models have deficiencies in water mass exchanges between the NE Atlantic and the NWES [27, 99] that is along the slope/shelf frontal zone (Fig. 1b). The open ocean and the deeper parts of the NWES become strongly stratified during summer. More focused climate change model runs, with increased resolution in the North Sea region, find that increased summer stratification will augment the reduction in onwelling. These processes have a potential to reduce biological production on the NWES by ~30% at the end of the twenty-first century [97]. On the other hand, a recent study [100] suggests that vertical mixing processes at the shelf break will maintain a connection to nutrient-enriched sub-pycnocline water masses in a future climate change scenario. This decoupling from the upper ocean conditions in the North Atlantic moderates the decline in new production projected by [97].

On the shallow part of the NWES, strong tidal currents persistently erode stratification and keep inner shelf waters permanently well-mixed. A tidal mixing front separates these well-mixed inner shelf waters from the seasonally stratified outer shelf waters [101]. Regional modeling of the NWES suggests that the cross-front exchanges are characterized by net on-shelf transports in the upper water layer and a net off-shelf transport to the lower layer of the outer shelf. This results in a net downwelling along the shelf [28]. Consequently, the projected increase and/or prolonged duration of summer stratification will reduce the degree of nutrient *onwelling* through nutrient depletion of upper layer outer shelf waters and thus amplify nutrient limitation on the near-shore well mixed water [28, 97].

3.1.2 Observations

Increasing recognition of the importance of the NE Atlantic for the North Sea ecosystem has motivated dedicated observational campaigns focused on the ocean–shelf interface, e.g., Fastnet and the UK Shelf Sea Biogeochemistry (SSB) Programme. Previous observations have shown that nutrient concentrations in the North Sea declined during the 1990s [96] primarily due to reduced oceanic *onwelling*, but also due to a reduction in the riverine nutrient loads to the southern domain. Also, the observed increase in northern North Sea nutrient concentrations during NAO+ phases has been explained by a combination of increased ocean-shelf water mass exchanges [29], decreased near-shelf stratification [94], and increased off-shelf winter MLD [95] (e.g., Sect. 2). Most previous nutrient observations have focused on nitrate and phosphate [93], although results from more recent surveys demonstrate that only silicate reaches limiting concentrations on the Hebridean shelf [102]. A mass balance approach suggests that 73% of the shelf water silicate must be resupplied from the open ocean in order to maintain shelf-wide estimates of productivity. This is considerably larger than similar estimates for nitrate (34%) and phosphate (28%) [102]. Although general aspects of the *onwelling* process apply to all major nutrients, we suggest that future research should pay more attention to silicate dynamics.

The stratification in the northern/deeper part of the North Sea intensified markedly between 2001 and 2002 and remained very strong during the following warm 2003–2005 period [103]. Apparent impacts of the intensified stratification on the phytoplankton concentration are here illustrated by seasonally-averaged near-surface chlorophyll (Chla) from ocean color satellites for the contrasting years, 2001 and 2002, respectively (Fig. 14). During 2001, Chla was highest on the shallower part of the NWES (<100 m depths, Fig. 14a) and much lower in deeper water. In contrast, during 2002, the near-shore Chla concentrations declined, while the Chla concentrations on the outer shelf/slope band from west of Ireland to north of Shetland increased significantly (Fig. 14b). This increase is particularly evident in the 100–200 m depth range, although also evident in the broader oceanic domain, e.g. the Faroe-Shetland Channel and the Norwegian Trench. It is plausible that the high Chla content in 2002 reflects a stratified and nutrient-depleted upper layer

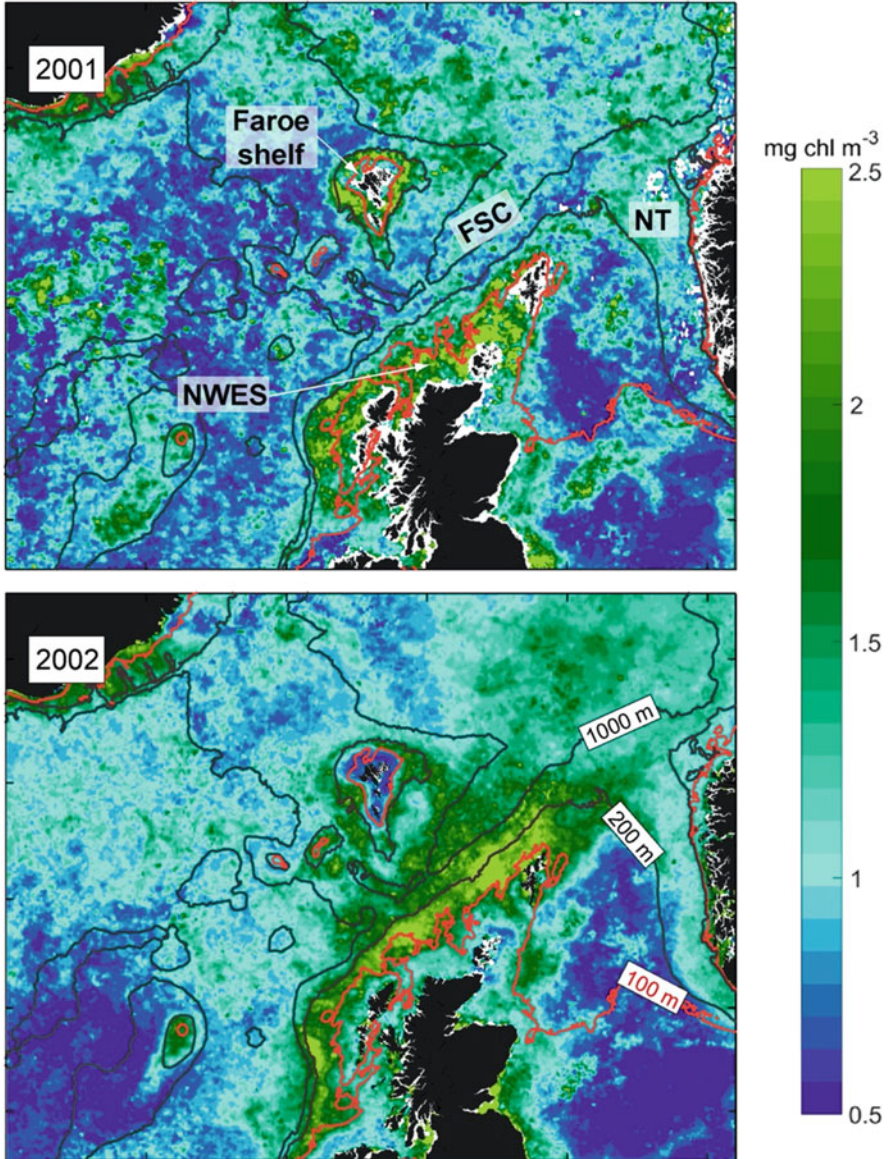


Fig. 14 Shift in phytoplankton concentrations from a year with weak stratification (2001, upper panel) to a year with strong stratification (2002, lower). The images are based on gridded near-surface satellite chlorophyll data, downloaded from the GlobColour Project, ACRI-ST (<http://www.globcolour.info>). Annual mean for the years 2001 and 2002 were computed from monthly averages of Level 3, merged (SeaWiFS, MODIS, MERIS), GSM-gridded [89] chlorophyll (CHL1) data on a 4-km horizontal grid from the months April–September. Abbreviations: Faroe-Shetland Channel (FSC), the Norwegian Trench (NT), and the NorthWestern European Slope (NWES)

containing a rich community of both large and small phytoplankton species, fueled by both new and regenerated production. Although the seasonally-averaged Chla concentration is not a robust proxy for primary production, the low shallow-shelf (<100 m) concentrations during 2002 do probably reflect reduced production. This could be caused by the low nutrient concentration in the onwelled outer shelf water, as discussed below (Sect. 3.2.3, Fig. 18c).

A significant reduction in landings of the key prey fish species – sand eel (*Ammodytes tobianus*) in 2003 [105] – also suggests that higher trophic level productivity in the northern North Sea might have decreased after 2002. The average landings of the period 1994–2002 was 880,000 tons whereas the average landings of the period 2003–2009 was only 288,000 tons. This period also coincided with a broad-scale breeding failure of the black-legged kittiwakes (*Rissa tridactyla*) in Britain [106].

The current level of understanding regarding impacts of *onwelling* to productivity of the North Sea is inherently limited by (a) the lack of detailed long-term observations and (b) the long stretch and openness of this system. Monitoring all key ocean-shelf exchange hotspots with adequate temporal resolution over decades might be an unfeasible task. Furthermore, fish and seabirds are relatively free to roam this large shelf region, rendering it difficult to trace how potential bottom-up processes propagate through the food web.

3.2 The Faroe Shelf

The upper layer water masses that flow northeastwards along the NWES also immerse the Faroe shelf, which is located centrally on the Iceland-Scotland Ridge (Fig. 1). In contrast to the NWES, the Faroe shelf is spatially confined in a manner that facilitates detailed observations of major ecosystem components. Comprehensive survey data at high spatial resolution and a large number of valuable time series are available from this system. And these span several decades and cover key aspects of phyto- and zooplankton communities, major fish stocks and seabird species [107–110]. The Faroe Shelf system therefore represents a good observational framework to examine impacts of *onwelling* on all major shelf ecosystem components – from nutrient-driven plankton dynamics to upper trophic levels. This system may thus serve as a useful model for understanding oceanic influence on boreal shelf systems in general.

The abovementioned 2001-to-2002 shift in the North Sea, from a productive inner shelf to a productive outer shelf/slope (and low inner shelf Chla concentrations) was more accentuated on the Faroe Shelf than on the NWES (Fig. 14). A previously defined Primary Production Index (PPI) for Faroese shelf waters [110] (Fig. 15) showed a major drop between 2001 and 2002. The PPI remained generally low until 2008, and these biologically poor conditions extended throughout all trophic levels on the Faroe shelf [108]. This period was also poor for seabirds, e.g., no fledged kittiwake chicks were observed at the Faroese colonies during this period [26].

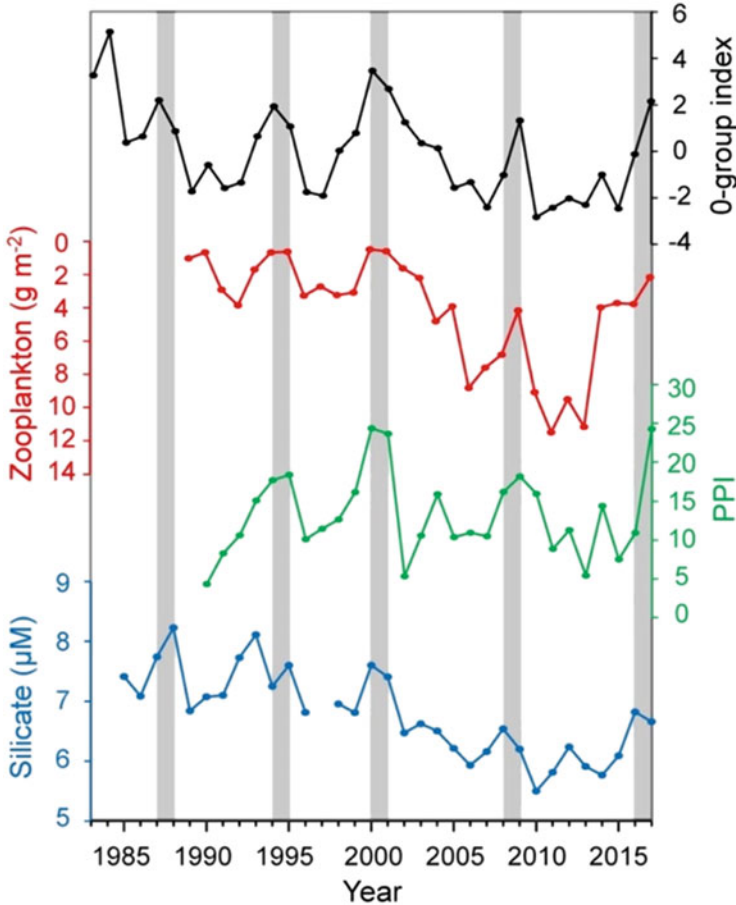


Fig. 15 Key ecological indicators for the Faroe shelf. Temporal development in the 0-group index estimated from four main fish stocks (black), zooplankton biomass in late June (red) (note the reversed axis), primary production index (PPI) from spring to late June (green), and open-ocean pre-bloom silicate concentrations (blue). The gray bars highlight convective (NAO+/SPG+) periods of simultaneous high 0-group index, low zooplankton biomass, high PPI, and high silicate concentration. From [60]

3.2.1 Primary Production Variability: Intensity and Phenology

Much effort has been dedicated to constrain the underlying mechanisms that govern the highly variable primary production on the Faroe shelf [108, 111, 112]. Here, cross-shelf front exchanges have been a central theme. Opposed to the view from the NWES, it has been hypothesized that increased exchanges may impede the primary production, since this might “flush” algae and spores off the shelf [111, 113]. These

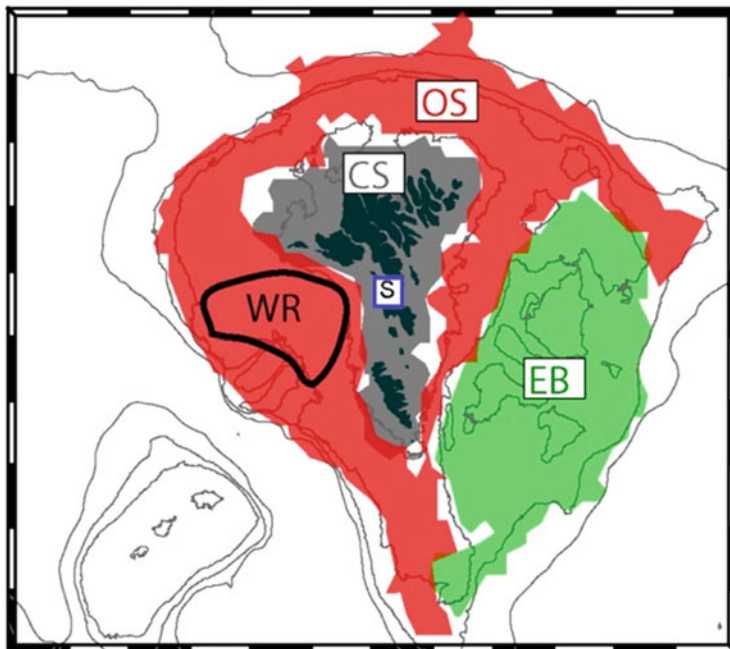


Fig. 16 The Faroe shelf bio-geographical zones: the Central Shelf (CS, gray), the Outer Shelf (OS, red) and the especially productive Western Region (WR), and the Eastern Banks (EB, green). The blue square shows station S. The 100 m, 200 m, 300 m, and 500 m isobaths are shown (from [104])

studies have, however, not explicitly considered variable stratification or the fact that the outer shelf/slope region also hosts a rich phytoplankton community.

The permanently well-mixed water on the central part of the shelf has been termed Faroe Shelf Water [114]. Eliassen et al. [32] showed that biomass observations at a fixed coastal Station (Station S, Fig. 16) provide a valid representation of the near-surface satellite-based Chla throughout the extent of the Central Shelf (CS) area. This is a region which roughly overlaps with the summer expanse of the Faroe Shelf Water domain (gray in Fig. 16). Phytoplankton biomass at Station S generally starts increasing during spring, however interrupted by halts in the Chla concentrations, apparent as local minima in the Chla time series [104] (Fig. 17).

Based on the phytoplankton concentration and phenology, observed from ocean color satellites, [104] have further divided the Faroe Plateau into the following three main bio-geographical zones: the Central Shelf (CS), the Eastern Banks (EB), and the Outer Shelf (OS) (Fig. 16). These non-overlapping regions cover the entire shelf within the 300 m isobath. Since the oceans, and in particular oceanic fronts, are dynamic, the borders of the zones should not be seen as rigid but merely as approximate positions with emphasis on summer conditions. Region CS blooms early, but Chla concentrations diminish quickly after the peak bloom, which

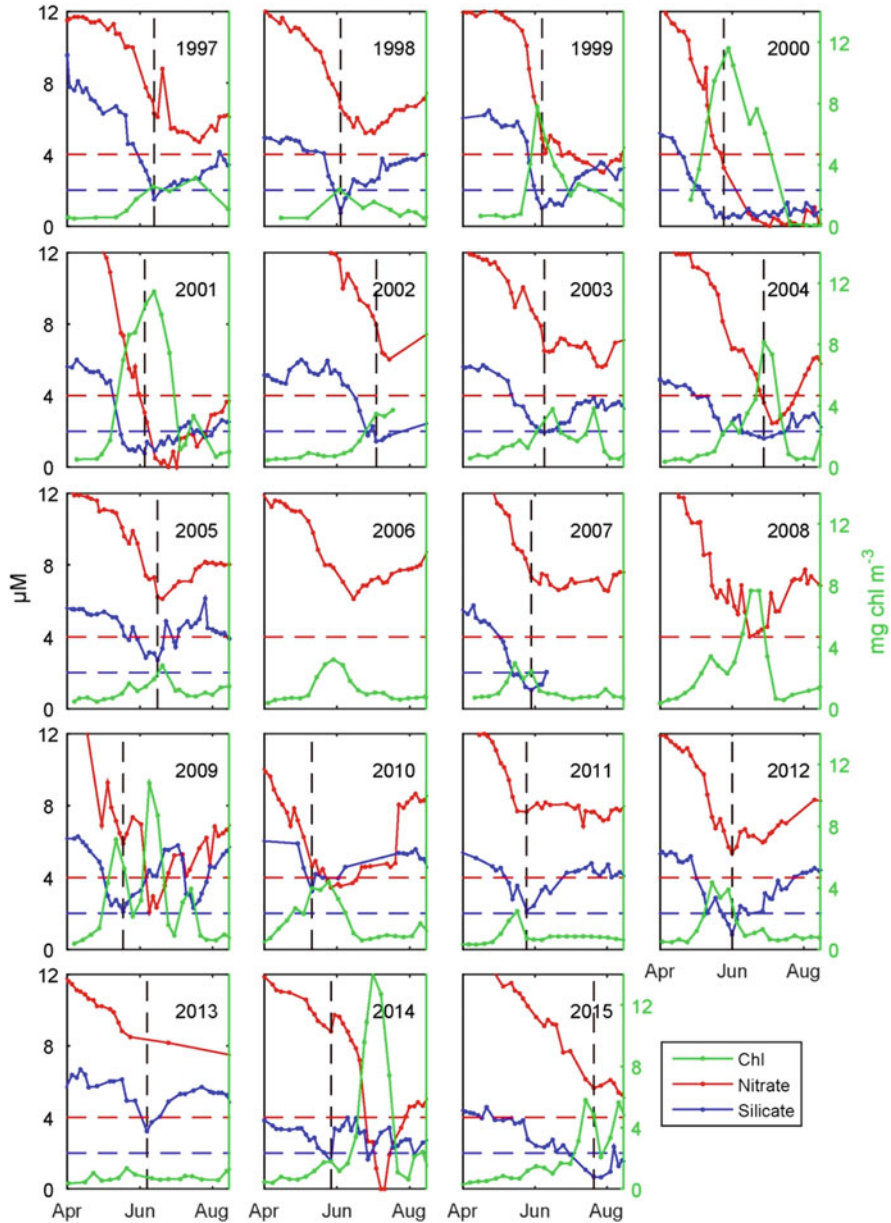


Fig. 17 Phytoplankton biomass (Chla) and nutrients from the coastal station S (see Fig. 16) on the Faroe shelf. The $2 \mu\text{M}$ and $4 \mu\text{M}$ lines are indicated as well as the date of the lowest observed silicate concentration (from [32]). The observations are made in water which is pumped from 18 m depth. This is located in a vertically and horizontally well-mixed Inner shelf, and the observations thus represent these shelf waters

typically takes place around late May–early June (Fig. 17). Chla concentrations remain relatively low during June and July, and in some years a short fall bloom occurs. The seasonally-averaged Chla concentration is lower in the CS compared to the surface layers in the surrounding waters during warm years (e.g., 2002, Fig. 14), when the stratification is generally intensified [103]. The OS blooms later than the CS, but the elevated Chla concentrations are sustained for a longer period. This region is therefore more visible in temporally averaged near-surface Chla images like in Figs. 11 and 14. Both studies by Eliassen et al. [104] and [32] highlighted the seasonally stratified western side of the OS – the Western Region (WR) (Fig. 16) – as a region which blooms relatively late, but which has the highest surface Chla concentrations on the Faroe Plateau during June–August.

A high-resolution (~1 km) version of the Hybrid Coordinate Ocean Model (HYCOM) [115] has been setup for the Faroese waters, and the output of key physical parameters compare favorably with in situ observations [116]. This model provides the first spatio-temporally comprehensive view of the stratification dynamics of the Faroe shelf. Similar to the NWES [117], a net *downwelling* is identified with net on-shelf transports from the upper OS-layer, and a net off-shelf transport from the CS to the lower OS-layer. Rasmussen et al. [116] presented the first discussion of the inter-annual primary production variability in the context of stratification. They showed that the growth-intensive years, 2000 and 2001, were also characterized by an early and sudden onset of stratification in the OS. Complementing the same HYCOM simulations with in situ oceanographic, atmospheric, and sunlight data, [118] explained the bloom timing by a *Critical Volume Hypothesis*. The onset of persistent OS stratification establishes a distinct tidal mixing front between the CS and the OS, which shifts shoreward during spring as the insolation and heat fluxes into the ocean strengthen. According to the *Critical Volume Hypothesis*, spring bloom initiates when the total primary production within the CS (which is shrinking at this point of the year) equals the net respiration of the same volume of water. The position of the tidal mixing front plays, in the horizontal *Critical Volume Hypothesis*, a role equivalent to the mixed layer depth in Sverdrup's classical (vertical) *Critical Depth Hypothesis* [118].

3.2.2 Silicate Limitation and Interplay Between the Outer and Central Shelf

Winter (pre-bloom) concentrations of nitrate and silicate on the Faroe Shelf are ~12 μM and ~5–7 μM , respectively (i.e., a Si:N ratio of ~1:2) [119, 120]. These concentrations have been declining since the early 1990s, in a similar manner as in the surrounding open ocean (Fig. 3) [52]. As mentioned, nutrient-related studies generally focus on nitrate, but since this nutrient only reaches limiting concentrations (< 4 μM) on the CS during the most productive years (e.g., 1994–1995, 2000–2001, 2004, 2009 and 2014 Figs. 15 and 17), nutrient dynamics have generally been overlooked in the early studies that examined bottom-up controls on inter-annual Faroe shelf bloom variability.

The average diatom ratio Si:N of 1.12 ± 0.33 [119] implies that silicate and nitrate should be taken up at approximately equal rates. Observations from the Faroe Shelf, together with those from the NWES [102], suggest that silicate limitation is equally, if not more, important for bloom dynamics in these shelf environments.

Maxima in the Chla concentrations for the CS typically occur after May and are associated with minima in silicate concentrations in 16 out of the 17-year time series (1997–2015; no silicate data for 2006 and 2008). In most cases (12 out of 17), silicate concentrations fall below $2 \mu\text{M}$ (Fig. 17) whereas it is, as mentioned, only the most productive years that nitrate concentrations are driven to limiting concentrations. From the end of May and throughout June, average silicate and nitrate concentrations, associated with Chla peaks, were in the range $1.9\text{--}2.2 \mu\text{M}$ and $5.0\text{--}7.1 \mu\text{M}$, respectively.

A main *onwelling* conduit to the CS originates from the upper layer WR [121], where the silicate concentrations are driven to even lower values than those on the CS [32]. After the first major CS Chla peak, when the environment has reached silicate limitation (Fig. 17), successive events between erosion/strengthening of the WR stratification and peaks/decreases in the CS Chla are observed [32]. This is idealistically sketched for a single de-stratification/re-stratification event in Fig. 18. The process is interpreted as follows: strong phytoplankton growth will quickly deplete the nutrients in the CS and in the upper WR layer, and nutrient supply will therefore be essential for the ongoing growth (Fig. 18c). The erosion of the established stratification leads to new nutrients from the bottom layer in the WR (green arrows in Fig. 18b) being supplied to the upper layer. If this nutrient input is not exhausted by growth in the outer shelf, it may help to maintain nutrient *onwelling* to the CS. Local and intermittent convection events will probably also admix nutrient-rich water from the lower layer directly onto the CS. The CS growth therefore alternates between nutrient enrichment by erosion of the pycnocline (Fig. 18a, b) and re-stratification and nutrient limitation (Fig. 18a, c). Phytoplankton dynamics on the species level have only been examined in 2004, 2005, and 2010 on the Faroe shelf. In these years a consistent shift from a community dominated by large diatoms to small/diatoms and flagellates has been observed when silicate concentrations reach $<2 \mu\text{M}$ [120, 122].

3.2.3 Higher Trophic Levels

Inter-annual variability in the size of fish larvae appears to be correlated with the primary production on the Faroe Shelf [60]. These authors have developed an *O-group index*, which is estimated from data on the four main fish stocks, cod (*Gadus morhua*), haddock (*Melanogrammus aeglefinus*), sand eel, and Norway pout (*Trisopterus esmarkii*), that together account for $>90\%$ of all the fish larvae on the shelf. The *O-group index* displays accentuated peaks every 7–10 years, which coincide with peaks in both the PPI and open ocean pre-bloom Si concentrations (Fig. 15). Jacobsen et al. [60] used the previously discussed silicate record from the northern Irminger Sea (Fig. 3) as a proxy for the open ocean surrounding the Faroe

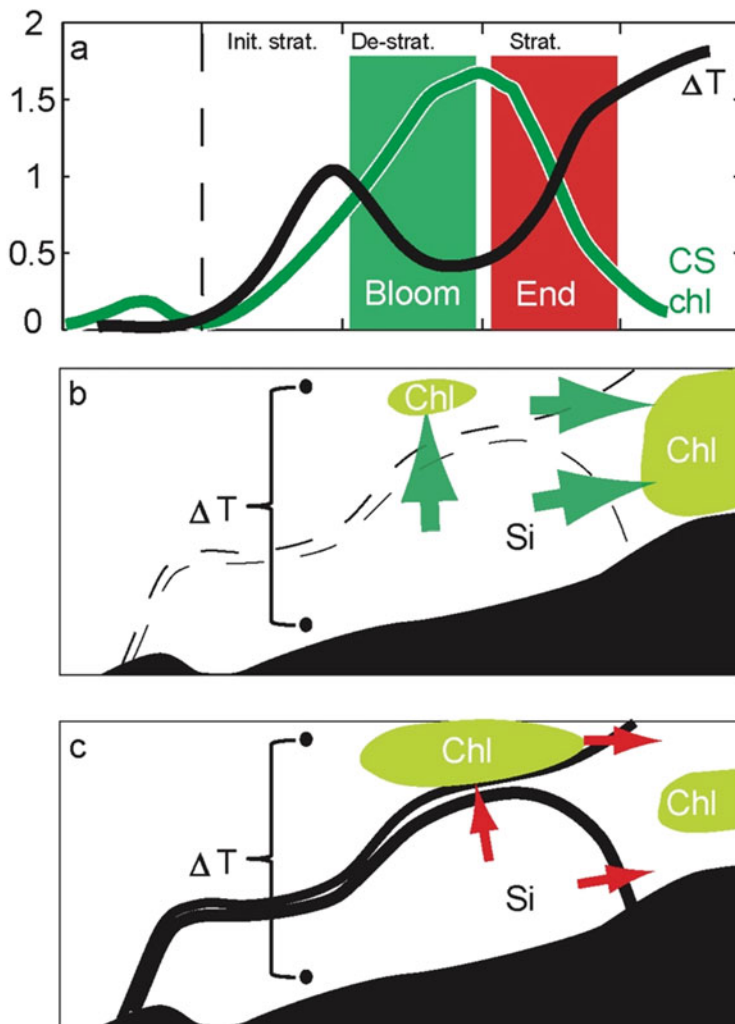


Fig. 18 An idealized sketch, describing the Faroe shelf bloom. (a) Time series of the temperature stratification (black) and Chla concentrations (green) on the western part of the outer shelf (the Western Region, see Fig. 16) and the Central Shelf (CS) and two idealized transects across the shelf during the green (b) and red phases (c), respectively. The red and green arrows symbolize small and large nutrient fluxes in the red and green phase (panel a), respectively, from the nutrient-rich “cold pool” (from [32])

shelf (Fig. 15). The relatively long record from the Irminger Sea is closely correlated to shorter records of pre-bloom silicate concentrations in the northern IB and north of the Faroes (not shown here).

The peaks associated with NAO+/SPG+ phases (Fig. 3) also concur with improved breeding success of the Faroe kittiwakes (*R. tridactyla*) [26] and improved recruitment and average weight gain of the main commercial fish stocks. Among many possible underlying mechanisms, we propose the following two as the most plausible:

1. NAO+/SPG+ dynamics are linked to oceanic Si peaks that fuel Faroe shelf primary production (PPI), which supports the growth of local zooplankton [123], key seabird fish-prey species (sand eel and Norway pout) and thus kittiwake chicks.
2. Increased volumes of zooplankton-rich subarctic water masses could increase the concentration of the copepod *C. finmarchicus* around the Faroe shelf. Thus, the on-shelf transport of eggs, nauplii, and adults of this key food item can increase, which in turn more directly supplies the fish and birds.

The impact on the kittiwakes could originate from the fact that these birds spend their non-breeding period, which is fall, winter, and early spring – and thus most of their lives – in the SPG region where they congregate near major oceanic frontal systems [16]. It has been shown that a strong gyre is associated with increased abundance of *C. finmarchicus* in the overwintering region in the Labrador and Irminger Sea [81]. It is therefore plausible that the improved non-breeding feeding conditions could translate to better breeding success the subsequent summer through a so-called carry-over effect [18, 26].

Finally, a similar SPG-shelf link, although focused on zooplankton, has been demonstrated for the south Iceland shelf. NAO+/SPG+ phases, associated with larger MLD in the northern Irminger Sea (Fig. 10), and northeastward-shifted SPG all coincide with markedly increased total zooplankton abundance on the south Iceland shelf during May (dominated by *C. finmarchicus*, [81]).

4 Summary

The fact that the North Atlantic subpolar gyre regulates temperature and salinity variability in the poleward flowing Atlantic water is now thoroughly described in the literature. It was, however, not until recently that awareness has been raised about the gyre's potential to also impact nutrient concentrations in the NE Atlantic. Subtropical waters are generally low in nutrients, but on their journey northwards they are being mixed with nutrient-rich subpolar waters – mainly along the frontal zones between the Atlantic and subarctic water masses. In years when the subpolar gyre circulation is intensified, more nutrients are upwelled from the nutrient-rich Intermediate Water level which forms the permanent pycnocline in the NE Atlantic. In contrast, when the gyre is weak, these *induction fluxes*, or *obduction*, are weak and nutrient-poor subtropical water masses become more prevalent in this region.

Silicate concentrations in the upper layer Atlantic waters have been decreasing since the early 1990s, likely linked to the declining subpolar gyre. This, in turn, was

associated with weaker winter overturning in the Labrador and Irminger Seas. The declining trend becomes identifiable in the vicinity of the Rockall-Hatton Plateau and extends downstream to the Nordic Seas (in north) and the Labrador Sea (in west). Here, we have suggested potential fertilization hotspots, located along the northeastern periphery of the subpolar gyre, and potential links to primary and secondary production, as well as the feeding migration of pelagic fish.

The gyre-regulated nutrient concentrations along the adjacent continental slopes will furthermore influence the ocean-to-shelf nutrient fluxes across shelf and tidal mixing fronts – the so-called nutrient *onwelling*. We review how this *onwelling* likely impacts the Northwestern European shelf seas and the North Sea and illustrate how variations in the nutrient *onwelling* propagate up through the food chain – using the Faroe shelf as a case study. We hypothesize that ecosystems on the south Iceland shelf, Faroe shelf, Northwestern European shelf seas, and potentially the Norwegian shelf are to some degree influenced by pre-bloom nutrient concentrations in the Atlantic-derived water masses that connect these regions. Our results from the spatially confined Faroe shelf, which are based on an extensive amount of observational data collected over more than two decades, could be important to the understanding of other larger shelf ecosystems as well. It is our recommendation that these observations are continued and complemented with additional observations of essential ocean variables both in the Faroes and at key locations on neighboring shelves (Table 2).

Table 2 List of acronyms, arranged as introduced in the text

| Acronyms | Name |
|----------|-----------------------------------|
| SPG | Subpolar gyre |
| SAF | Subarctic Front |
| NAC | North Atlantic Current |
| RTB | Rockall Trough Branch |
| SAFB | Sub-Arctic Front Branch |
| CIBB | Central Iceland Basin Branch |
| IFF | Iceland-Faroe Front |
| MLD | Mixed Layer Depth |
| AMO | Atlantic Multidecadal Oscillation |
| NAO | North Atlantic Oscillation |
| GSA | Great Salinity Anomaly |
| IB | Iceland Basin |
| SSH | Sea-surface height |
| Si | Silicate |
| NWES | Northwestern European slope |
| PPI | Primary Production Index |
| CS | Central Shelf |
| EB | Eastern Banks |
| OS | Outer Shelf |
| WR | Western Region |

References

1. Trenkel VM, Huse G, MacKenzie BR, Alvarez P, Arrizabalaga H, Castonguay M, Goñi N, Grégoire F, Hátún H, Jansen T, Jacobsen JA, Lehodey P, Lutcavage M, Mariani P, Melvin GD, Neilson JD, Nøttestad L, Óskarsson GJ, Payne MR, Richardson DE, Senina I, Speirs DC (2014) Comparative ecology of widely distributed pelagic fish species in the North Atlantic: implications for modelling climate and fisheries impacts. *Prog Oceanogr* 129:219–243. <https://doi.org/10.1016/j.pocean.2014.04.030>
2. Sundby S (2000) Recruitment of Atlantic cod stocks in relation to temperature and advection of copepod populations. *Sarsia* 85:277–298. <https://doi.org/10.1080/00364827.2000.10414580>
3. Frederiksen M, Moe B, Daunt F, Phillips RA, Barrett RT, Bogdanova MI, Boulinier T, Chardine JW, Chastel O, Chivers LS, Christensen-Dalsgaard S, Clément-Chastel C, Colhoun K, Freeman R, Gaston AJ, González-Solís J, Goutte A, Grémillet D, Guilford T, Jensen GH, Krasnov Y, Lorentsen SH, Mallory ML, Newell M, Olsen B, Shaw D, Steen H, Strøm H, Systad GH, Thórarinnsson TL, Anker-Nilssen T (2011) Multicolony tracking reveals the winter distribution of a pelagic seabird on an ocean basin scale. *Divers Distrib* 18:530–542. <https://doi.org/10.1111/j.1472-4642.2011.00864.x>
4. Wanless S, Frederiksen M, Daunt F, Scott BE, Harris MP (2007) Black-legged kittiwakes as indicators of environmental change in the North Sea: evidence from long-term studies. *Prog Oceanogr* 72:30–38. <https://doi.org/10.1016/j.pocean.2006.07.007>
5. Jansen T, Campbell A, Kelly C, Hátún H, Payne MR (2012) Migration and fisheries of north east Atlantic mackerel (*Scomber scombrus*) in autumn and winter. *PLoS One* 7(12):e51541. <https://doi.org/10.1371/journal.pone.0051541>
6. Mackenzie BR, Payne MR, Boje J, Høyer JL, Siegstad H (2014) A cascade of warming impacts brings bluefin tuna to Greenland waters. *Glob Chang Biol* 20:2484–2491. <https://doi.org/10.1111/gcb.12597>
7. Lalli CM, Parsons TR (1997) Biological oceanography: an introduction. 2nd edn. Elsevier, Oxford, pp 1–309
8. Longhurst A (2006) Ecological geography of the sea. 2nd edn. Academic Press, London, pp 1–541
9. Mahadevan A, D'Asaro E, Lee C, Perry MJ (2012) Eddy-driven stratification initiates North Atlantic spring phytoplankton blooms. *Science* 337:54–58. <https://doi.org/10.1126/science.1218740>
10. Chiswell SM, Calil PHR, Boyd PW (2015) Spring blooms and annual cycles of phytoplankton: a unified perspective. *J Plankton Res* 37:500–508. <https://doi.org/10.1093/plankt/fbv021>
11. Allen JT, Brown L, Sanders R, Moore CM, Mustard A, Fielding S, Lucas M, Rixen M, Savidge G, Henson S, Mayor D (2005) Diatom carbon export enhanced by silicate upwelling in the northeast Atlantic. *Nature* 437:728–732. <https://doi.org/10.1038/nature03948>
12. Henson SA, Robinson I, Allen JT, Waniek JJ (2006) Effect of meteorological conditions on interannual variability in timing and magnitude of the spring bloom in the Irminger Basin, North Atlantic. *Deep-Sea Res Part I* 53:1601–1615. <https://doi.org/10.1016/j.dsr.2006.07.009>
13. Egge JK, Aksnes DL (1992) Silicate as regulating nutrient in phytoplankton competition. *Mar Ecol Prog Ser* 83:281–289. <https://doi.org/10.3354/meps083281>
14. Nielsdóttir MC, Moore CM, Sanders R, Hinz DJ, Achterberg EP (2009) Iron limitation of the postbloom phytoplankton communities in the Iceland Basin. *Global Biogeochem Cycles* 23:GB3001. <https://doi.org/10.1029/2008GB003410>
15. Meyer-Harms B, Irigoien X, Head R, Harris R (1999) Selective feeding on natural phytoplankton by *Calanus finmarchicus* before, during, and after the 1997 spring bloom in the Norwegian Sea. *Limnol Oceanogr* 44:154–165. <https://doi.org/10.4319/lo.1999.44.1.0154>
16. Pacariz SV, Hátún H, Jacobsen JA, Johnson C, Eliassen S, Rey F (2016) Nutrient-driven poleward expansion of the Northeast Atlantic mackerel (*Scomber scombrus*) stock: a new hypothesis. *Elem Sci Anthr* 4:000105. <https://doi.org/10.12952/journal.elementa.000105>

17. Edwards EWJ, Quinn LR, Wakefield ED, Miller PI, Thompson PM (2013) Tracking a northern fulmar from a Scottish nesting site to the Charlie-Gibbs fracture zone: evidence of linkage between coastal breeding seabirds and Mid-Atlantic Ridge feeding sites. *Deep-Sea Res Part II Top Stud Oceanogr* 98:438–444. <https://doi.org/10.1016/j.dsr2.2013.04.011>
18. Bogdanova MI, Daunt F, Newell M, Phillips RA, Harris MP, Wanless S (2011) Seasonal interactions in the black-legged kittiwake, *Rissa tridactyla*: links between breeding performance and winter distribution. *Proc R Soc B Biol Sci* 278:2412–2418. <https://doi.org/10.1098/rspb.2010.2601>
19. Holliday NP (2003) Air-sea interaction and circulation changes in the northeast Atlantic. *J Geophys Res* 108(C8):3259. <https://doi.org/10.1029/2002JC001344>
20. Bersch M, Meincke J, Sy A (1999) Interannual thermohaline changes in the northern North Atlantic 1991–1996. *Deep-Sea Res Part II Top Stud Oceanogr* 46:55–75. [https://doi.org/10.1016/S0967-0645\(98\)00114-3](https://doi.org/10.1016/S0967-0645(98)00114-3)
21. Ullgren JE, Fer I, Darelus E, Beard N (2014) Interaction of the Faroe Bank Channel overflow with Iceland Basin intermediate waters. *J Geophys Res Oceans* 119:228–240. <https://doi.org/10.1002/2013JC009437>
22. Hátún H, Chafik L (2018) On the recent ambiguity of the North Atlantic subpolar gyre index. *J Geophys Res Oceans* 123:5072–5076. <https://doi.org/10.1029/2018JC014101>
23. Sandø AB, Furevik T (2008) Relation between the wind stress curl in the North Atlantic and the Atlantic inflow to the Nordic seas. *J Geophys Res* 113:C06028. <https://doi.org/10.1029/2007JC004236>
24. Hátún H, Sandø AB, Drange H, Hansen B, Valdimarsson H (2005) Influence of the Atlantic subpolar gyre on the thermohaline circulation. *Science* 309:1841–1844. <https://doi.org/10.1126/science.1114777>
25. Brambilla E, Talley LD (2008) Subpolar mode water in the northeastern Atlantic: 1. Averaged properties and mean circulation. *J Geophys Res Ocean* 113:C04025. <https://doi.org/10.1029/2006JC004062>
26. Hátún H, Olsen B, Pacariz SV (2017) The dynamics of the North Atlantic subpolar gyre introduces predictability to the breeding success of kittiwakes. *Front Mar Sci* 4:123. <https://doi.org/10.3389/fmars.2017.00123>
27. Mathis M, Elizalde A, Mikolajewicz U (2018) Which complexity of regional climate system models is essential for downscaling anthropogenic climate change in the Northwest European Shelf? *Clim Dyn* 50:2637–2659. <https://doi.org/10.1007/s00382-017-3761-3>
28. Holt J, Butenschön M, Wakelin SL, Artioli Y, Allen JI (2012) Oceanic controls on the primary production of the northwest European continental shelf: model experiments under recent past conditions and a potential future scenario. *Biogeosciences* 9:97–117. <https://doi.org/10.5194/bg-9-97-2012>
29. Emeis K-C, Beusekom JV, Callies U, Ebinghaus R, Kannen A, Kraus G, Kröncke I, Lenhart H, Lorkowski I, Matthias V, Möllmann C, Pätsch J, Scharfe M, Thomas H, Weisse R, Zorita E (2015) The North Sea — a shelf sea in the Anthropocene. *J Mar Syst* 141:18–33. <https://doi.org/10.1016/j.jmarsys.2014.03.012>
30. Gröger M, Maier-Reimer E, Mikolajewicz U, Moll A, Sein D (2013) NW European shelf under climate warming: implications for open ocean – shelf exchange, primary production, and carbon absorption. *Biogeosciences* 10:3767–3792. <https://doi.org/10.5194/bg-10-3767-2013>
31. Pätsch J, Kühn W (2008) Nitrogen and carbon cycling in the North Sea and exchange with the North Atlantic—a model study. Part I. nitrogen budget and fluxes. *Cont Shelf Res* 28:767–787. <https://doi.org/10.1016/j.csr.2007.12.013>
32. Eliassen SK, Hátún H, Larsen KMH, Jacobsen S (2017) Faroe shelf bloom phenology – the importance of ocean-to-shelf silicate fluxes. *Cont Shelf Res* 143:43–53. <https://doi.org/10.1016/j.csr.2017.06.004>

33. Williams RG, Follows MJ (2003) Physical transport of nutrients and the maintenance of biological production. In: *Ocean biogeochemistry*. Springer, Berlin, pp 19–51. https://doi.org/10.1007/978-3-642-55844-3_3
34. McCartney MS (1992) Recirculating components to the deep boundary current of the northern North Atlantic. *Prog Oceanogr* 29:283–383. [https://doi.org/10.1016/0079-6611\(92\)90006-L](https://doi.org/10.1016/0079-6611(92)90006-L)
35. Arhan M (1990) The North-Atlantic current and SubArctic intermediate water. *J Mar Res* 48:109–144. <https://doi.org/10.1357/002224090784984605>
36. Bersch M (2002) North Atlantic oscillation–induced changes of the upper layer circulation in the northern North Atlantic Ocean. *J Geophys Res* 107(C10):3156. <https://doi.org/10.1029/2001JC000901>
37. Wade IP, Ellett DJ, Heywood KJ (1997) The influence of intermediate waters on the stability of the eastern North Atlantic. *Deep-Sea Res Part I Oceanogr Res Pap* 44:1405–1426. [https://doi.org/10.1016/S0967-0637\(97\)00023-X](https://doi.org/10.1016/S0967-0637(97)00023-X)
38. Johnson C, Inall M, Häkkinen S (2013) Declining nutrient concentrations in the northeast Atlantic as a result of a weakening subpolar gyre. *Deep-Sea Res Part I Oceanogr Res Pap* 82:95–107. <https://doi.org/10.1016/j.dsr.2013.08.007>
39. McCartney MS, Talley LD (1982) The sub-polar mode water of the North-Atlantic Ocean. *J Phys Oceanogr* 12:1169–1188. [https://doi.org/10.1175/1520-0485\(1982\)012<1169:TSMWOT>2.0.CO;2](https://doi.org/10.1175/1520-0485(1982)012<1169:TSMWOT>2.0.CO;2)
40. Brambilla E, Talley LD, Robbins PE (2008) Subpolar mode water in the northeastern Atlantic: 2. Origin and transformation. *J Geophys Res Oceans* 113:C04026. <https://doi.org/10.1029/2006JC004063>
41. Talley LD, McCartney MS (1982) Distribution and circulation of Labrador Sea water. *J Phys Oceanogr* 12:1189–1205. [https://doi.org/10.1175/1520-0485\(1982\)012<1189:DACOLS>2.0.CO;2](https://doi.org/10.1175/1520-0485(1982)012<1189:DACOLS>2.0.CO;2)
42. Van Aken HM, Becker G (1996) Hydrography and through-flow in the north-eastern North Atlantic Ocean: the NANSEN project. *Prog Oceanogr* 38:297–346. [https://doi.org/10.1016/S0079-6611\(97\)00005-0](https://doi.org/10.1016/S0079-6611(97)00005-0)
43. Thomas LN, Joyce TM (2010) Subduction on the northern and southern flanks of the Gulf stream. *J Phys Oceanogr* 40:429–438. <https://doi.org/10.1175/2009JPO4187.1>
44. Sarafanov A (2009) On the effect of the North Atlantic oscillation on temperature and salinity of the subpolar North Atlantic intermediate and deep waters. *ICES J Mar Sci* 66:1448–1454. <https://doi.org/10.1093/icesjms/fsp094>
45. Sarafanov A, Mercier H, Falina A, Sokov A (2010) Cessation and partial reversal of deep water freshening in the northern North Atlantic: observation-based estimates and attribution. *Tellus A Dynamic Meteorol Oceanogr* 62:80–90. <https://doi.org/10.1111/j.1600-0870.2009.00418.x>
46. Hurrell JW (1995) Decadal trends in the North-Atlantic oscillation: regional temperatures and precipitation. *Science* 269:676–679. <https://doi.org/10.1126/science.269.5224.676>
47. Häkkinen S, Rhines PB (2004) Decline of subpolar North Atlantic circulation during the 1990s. *Science* 304:555–559. <https://doi.org/10.1126/science.1094917>
48. Larsen KMH, Hátún H, Hansen B, Kristiansen R (2012) Atlantic water in the Faroe area: sources and variability. *ICES J Mar Sci* 69:802–808. <https://doi.org/10.1093/icesjms/fss028>
49. Goldenberg SB, Landsea CW, Mestas-Nunez AM, Gray WM (2001) The recent increase in Atlantic hurricane activity: causes and implications. *Science* 293:474–479. <https://doi.org/10.1126/science.1060040>
50. de Boisséson E, Thierry V, Mercier H, Caniaux G, Desbruyères D (2012) Origin, formation and variability of the subpolar mode water located over the Reykjanes Ridge. *J Geophys Res* 117:C12005. <https://doi.org/10.1029/2011JC007519>
51. Rey F (2012) Declining silicate concentrations in the Norwegian and Barents Seas. *ICES J Mar Sci* 69:208–212. <https://doi.org/10.1093/icesjms/fss007>
52. Hátún H, Azetsu-Scott K, Somavilla R, Rey F, Johnson C, Mathis M, Mikolajewicz U, Coupel P, Tremblay J-É, Hartman S, Pacariz SV, Salter I, Ólafsson J (2017) The subpolar

- gyre regulates silicate concentrations in the North Atlantic. *Sci Rep* 7:14576. <https://doi.org/10.1038/s41598-017-14837-4>
53. Ilyina T, Six KD, Segsneider J, Maier-Reimer E, Li H, Núñez-Riboni I (2013) Global Ocean biogeochemistry model HAMOCC: model architecture and performance as component of the MPI-Earth system model in different CMIP5 experimental realizations. *J Adv Model Earth Syst* 5:287–315. <https://doi.org/10.1029/2012MS000178>
 54. Stando I, Kieke D, Rhein M, Gruber N, Steinfeldt R (2015) Interannual to decadal oxygen variability in the mid-depth water masses of the eastern North Atlantic. *Deep-Sea Res Part I Oceanogr Res Pap* 95:85–98. <https://doi.org/10.1016/j.dsr.2014.10.009>
 55. Bower AS, Le Cann B, Rossby T, Zenk W, Gould J, Speer K, Richardson PL, Prater MD, Zhang H-M (2002) Directly measured mid-depth circulation in the northeastern North Atlantic Ocean. *Nature* 419:603–607. <https://doi.org/10.1038/nature01078>
 56. McGrath T, Nolan G, McGovern E (2012) Chemical characteristics of water masses in the Rockall Trough. *Deep Sea Res Part I Oceanogr Res Pap* 61:57–73. <https://doi.org/10.1016/j.dsr.2011.11.007>
 57. Dickson RR, Meincke J, Malmberg SA, Lee AJ (1988) The great salinity anomaly in the northern North-Atlantic 1968-1982. *Prog Oceanogr* 20:103–151. [https://doi.org/10.1016/0079-6611\(88\)90049-3](https://doi.org/10.1016/0079-6611(88)90049-3)
 58. Belkin IM (2004) Propagation of the “great salinity anomaly” of the 1990s around the northern North Atlantic. *Geophys Res Lett* 31:L08306. <https://doi.org/10.1029/2003GL019334>
 59. Holliday NP, Bersch M, Berx B, Chafik L, Cunningham S, Florindo-López C, Hátún H, Johns W, Josey SA, Larsen KMH, Mulet S, Oltmanns M, Reverdin G, Rossby T, Thierry V, Valdimarsson H, Yashayaev I (2020) Ocean circulation causes the largest freshening event for 120 years in eastern subpolar North Atlantic. *Nat Commun* 11:585. <https://doi.org/10.1038/s41467-020-14474-y>
 60. Jacobsen S, Gaard E, Hátún H, Steingrund P, Larsen KMH, Reinert J, Ólafsdóttir SR, Poulsen M, Vang HBM (2019) Environmentally driven ecological fluctuations on the Faroe shelf revealed by fish juvenile surveys. *Front Mar Sci* 6:559. <https://doi.org/10.3389/fmars.2019.00559>
 61. Hansen B, Østerhus S (2000) North Atlantic–Nordic Seas exchanges. *Prog Oceanogr* 45:109–208. [https://doi.org/10.1016/S0079-6611\(99\)00052-X](https://doi.org/10.1016/S0079-6611(99)00052-X)
 62. Childers KH, Flagg CN, Rossby T, Schrum C (2015) Directly measured currents and estimated transport pathways of Atlantic water between 59.5°N and the Iceland-Faroes-Scotland Ridge. *Tellus A Dyn Meteorol Oceanogr* 67:28067. <https://doi.org/10.3402/tellusa.v67.28067>
 63. Sarafanov A, Falina A, Sokov A, Demidov A (2008) Intense warming and salinification of intermediate waters of southern origin in the eastern subpolar North Atlantic in the 1990s to mid-2000s. *J Geophys Res* 113:C12022. <https://doi.org/10.1029/2008JC004975>
 64. Van Aken HM, De Boer CJ (1995) On the synoptic hydrography of intermediate and deep-water masses in the Iceland Basin. *Deep-Sea Res Part I Oceanogr Res Pap* 42:165–189. [https://doi.org/10.1016/0967-0637\(94\)00042-Q](https://doi.org/10.1016/0967-0637(94)00042-Q)
 65. Beaird NL, Rhines PB, Eriksen CC (2016) Observations of seasonal subduction at the Iceland-Faroe front. *J Geophys Res Oceans* 121:4026–4040. <https://doi.org/10.1002/2015JC011501>
 66. Pollard RT, Read JF, Holliday NP, Leach H (2004) Water masses and circulation pathways through the Iceland Basin during Vivaldi 1996. *J Geophys Res* 109:C04004. <https://doi.org/10.1029/2003JC002067>
 67. Bersch M, Yashayaev I, Koltermann KP (2007) Recent changes of the thermohaline circulation in the subpolar North Atlantic. *Ocean Dyn* 57:223–235. <https://doi.org/10.1007/s10236-007-0104-7>
 68. Seim KS, Fer I (2011) Mixing in the stratified interface of the Faroe Bank Channel overflow: the role of transverse circulation and internal waves. *J Geophys Res Oceans* 116:C07022. <https://doi.org/10.1029/2010JC006805>
 69. Darelius E, Fer I, Quadfasel D (2011) Faroe Bank Channel overflow: mesoscale variability. *J Phys Oceanogr* 41:2137–2154. <https://doi.org/10.1175/JPO-D-11-035.1>

70. Darelius E, Ullgren JE, Fer I (2013) Observations of Barotropic oscillations and their influence on mixing in the Faroe Bank Channel overflow region. *J Phys Oceanogr* 43:1525–1532. <https://doi.org/10.1175/JPO-D-13-059.1>
71. Beaird NL, Fer I, Rhines P, Eriksen C (2012) Dissipation of turbulent kinetic energy inferred from seagliders: an application to the eastern Nordic Seas overflows. *J Phys Oceanogr* 42:2268–2282. <https://doi.org/10.1175/JPO-D-12-094.1>
72. Bringedal C, Eldevik T, Skagseth Ø, Spall MA, Østerhus S (2018) Structure and forcing of observed exchanges across the Greenland–Scotland ridge. *J Clim* 31:9881–9901. <https://doi.org/10.1175/JCLI-D-17-0889.1>
73. Yang J, Pratt LJ (2013) On the effective capacity of the dense-water reservoir for the Nordic seas overflow: some effects of topography and wind stress. *J Phys Oceanogr* 43:418–431. <https://doi.org/10.1175/JPO-D-12-087.1>
74. Chafik L, Hátún H, Kjellsson J, Larsen KMH, Rossby T, Berx B (2020) Discovery of an unrecognized pathway carrying overflow waters toward the Faroe Bank Channel. *Nat Commun* 11:3721. <https://doi.org/10.1038/s41467-020-17426-8>
75. Johnson GC, Gruber N (2007) Decadal water mass variations along 20°W in the northeastern Atlantic Ocean. *Prog Oceanogr* 73:277–295. <https://doi.org/10.1016/j.pocean.2006.03.022>
76. de Jong MF, de Steur L (2016) Strong winter cooling over the Irminger Sea in winter 2014–2015, exceptional deep convection, and the emergence of anomalously low SST. *Geophys Res Lett* 43:7106–7113. <https://doi.org/10.1002/2016GL069596>
77. Yashayaev I, Loder JW (2016) Recurrent replenishment of Labrador Sea water and associated decadal-scale variability. *J Geophys Res Oceans* 121:8095–8114. <https://doi.org/10.1002/2016JC012046>
78. Crockett KC, Hill E, Abell RE, Johnson C, Gary SF, Brand T, Hathorne EC (2018) Rare earth element distribution in the NE Atlantic: evidence for benthic sources, longevity of the seawater signal, and biogeochemical cycling. *Front Mar Sci* 5:147. <https://doi.org/10.3389/fmars.2018.00147>
79. Richter K, Maus S (2011) Interannual variability in the hydrography of the Norwegian Atlantic current: frontal versus advective response to atmospheric forcing. *J Geophys Res* 116:C12031. <https://doi.org/10.1029/2011JC007311>
80. Siegismund F, Johannessen J, Drange H, Mork KA, Korablev A (2007) Steric height variability in the Nordic seas. *J Geophys Res Oceans* 112:C12010. <https://doi.org/10.1029/2007JC004221>
81. Hátún H, Lohmann K, Matei D, Jungclauss JH, Pacariz S, Bersch M, Gislason A, Ólafsson J, Reid PC (2016) An inflated subpolar gyre blows life toward the northeastern Atlantic. *Prog Oceanogr* 147:49–66. <https://doi.org/10.1016/j.pocean.2016.07.009>
82. Frajka-Williams E, Rhines PB, Eriksen CC (2009) Physical controls and mesoscale variability in the Labrador Sea spring phytoplankton bloom observed by Seaglider. *Deep-Sea Res I* 56:2144–2161. <https://doi.org/10.1016/j.dsr.2009.07.008>
83. Hátún H, Eriksen CC, Rhines PB (2007) Buoyant eddies entering the Labrador Sea observed with gliders and altimetry. *J Phys Oceanogr* 37:2838–2854. <https://doi.org/10.1175/2007JPO3567.1>
84. Alkire MB, D’Asaro E, Lee C, Perry MJ, Gray A, Cetinić I, Briggs N, Rehm E, Kallin E, Kaiser J, González-Posada A (2012) Estimates of net community production and export using high-resolution, Lagrangian measurements of O₂, NO₃⁻, and POC through the evolution of a spring diatom bloom in the North Atlantic. *Deep Sea Res Part I Oceanogr Res Pap* 64:157–174. <https://doi.org/10.1016/j.dsr.2012.01.012>
85. Painter SC, Henson SA, Forryan A, Steigenberger S, Klar J, Stinchcombe MC, Rogan N, Baker AR, Achterberg EP, Moore CM (2014) An assessment of the vertical diffusive flux of iron and other nutrients to the surface waters of the subpolar North Atlantic Ocean. *Biogeosciences* 11:2113–2130. <https://doi.org/10.5194/bg-11-2113-2014>
86. Lankhorst M, Zenk W (2006) Lagrangian observations of the middepth and deep velocity fields of the northeastern Atlantic Ocean. *J Phys Oceanogr* 36:43–63. <https://doi.org/10.1175/JPO2869.1>

87. Gudfinnsson H, Debes H, Falkenhaug T, Gaard E, Gislason A, Petursdottir H, Sigurdsson T, Stupnikova A, Valdimarsson H (2008) Abundance and productivity of the pelagic ecosystem across the northern Mid-Atlantic Ridge in June 2003. ICES CM2008/C:12
88. ICES (2020) Working group on widely distributed stocks (WGWISE). ICES Sci Rep 2 (82):1019. <https://doi.org/10.17895/ices.pub.7475>
89. Maritorena S, d'Andon OHF, Mangin A, Siegel DA (2010) Merged satellite ocean color data products using a bio-optical model: characteristics, benefits and issues. Remote Sens Environ 114:1791–1804. <https://doi.org/10.1016/j.rse.2010.04.002>
90. Langøy H, Nøttestad L, Skaret G, Broms C, Fernö A (2012) Overlap in distribution and diets of Atlantic mackerel (*Scomber scombrus*), Norwegian spring-spawning herring (*Clupea harengus*) and blue whiting (*Micromesistius poutassou*) in the Norwegian Sea during late summer. Mar Biol Res 8:442–460. <https://doi.org/10.1080/17451000.2011.642803>
91. Ogi M, Yamazaki K, Tachibana Y (2004) The summertime annular mode in the northern hemisphere and its linkage to the winter mode. J Geophys Res 109:D20114. <https://doi.org/10.1029/2004JD004514>
92. Waniek JJ, Holliday NP (2006) Large-scale physical controls on phytoplankton growth in the Irminger Sea, part II: model study of the physical and meteorological preconditioning. J Mar Syst 59:219–237. <https://doi.org/10.1016/j.jmarsys.2005.10.005>
93. Galloway JN, Howarth RW, Michaels AF, Nixon SW, Prospero JM, Dentener FJ (1996) Nitrogen and phosphorus budgets of the North Atlantic Ocean and its watershed. Biogeochemistry 35:3–25. <https://doi.org/10.1007/BF02179823>
94. Holt J, Schrum C, Cannaby H, Daewel U, Allen I, Artioli Y, Bopp L, Butenschon M, Fach BA, Harle J, Pushpadas D, Salihoglu B, Wakelin S (2016) Potential impacts of climate change on the primary production of regional seas: a comparative analysis of five European seas. Prog Oceanogr 140:91–115. <https://doi.org/10.1016/j.pocean.2015.11.004>
95. Steinacher M, Joos F, Frölicher TL, Bopp L, Cadule P, Cocco V, Doney SC, Gehlen M, Lindsay K, Moore JK, Schneider B, Segsneider J (2010) Projected 21st century decrease in marine productivity: a multi-model analysis. Biogeosciences 7:979–1005. <https://doi.org/10.5194/bg-7-979-2010>
96. Vermaat JE, McQuatters-gollop A, Eleveld MA, Gilbert AJ (2008) Past, present and future nutrient loads of the North Sea: causes and consequences. Estuar Coast Shelf Sci 80:53–59. <https://doi.org/10.1016/j.ecss.2008.07.005>
97. Gröger M, Maier-Reimer E, Mikolajewicz U, Moll A, Sein D (2013) NW European shelf under climate warming: implications for open ocean - shelf exchange, primary production, and carbon absorption. Biogeosciences 10:3767–3792. <https://doi.org/10.5194/bg-10-3767-2013>
98. IPCC (2019) IPCC special report on the ocean and cryosphere in a changing climate. <https://www.ipcc.ch/srocc/cite-report/>
99. Holt J, Allen JI, Anderson TR, Brewin R, Butenschön M, Harle J, Huse G, Lehodey P, Lindemann C, Memery L, Salihoglu B, Senina I, Yool A (2014) Challenges in integrative approaches to modelling the marine ecosystems of the North Atlantic: physics to fish and coasts to ocean. Prog Oceanogr 129:285–313. <https://doi.org/10.1016/j.pocean.2014.04.024>
100. Mathis M, Elizalde A, Mikolajewicz U (2019) The future regime of Atlantic nutrient supply to the Northwest European Shelf. J Mar Syst 189:98–115. <https://doi.org/10.1016/j.jmarsys.2018.10.002>
101. Sharples J, Holt J, Dye SR (2013) Impacts of climate change on shelf sea stratification. MCCCIP Sci Rev:67–70. <https://doi.org/10.14465/2013.arc08.067-070>
102. Painter SC, Hartman SE, Kivimäe C, Salt LA, Clargo NM, Daniels CJ, Bozec Y, Daniels L, Allen S, Hemsley VS, Moschonas G, Davidson K (2017) The elemental stoichiometry (C, Si, N, P) of the Hebrides Shelf and its role in carbon export. Prog Oceanogr 159:154–177. <https://doi.org/10.1016/j.pocean.2017.10.001>
103. Pätsch J, Burchard H, Dieterich C, Gräwe U, Gröger M, Mathis M, Kapitza H, Bersch M, Moll A, Pohlmann T, Su J, Ho-hagemann HTM, Schulz A, Elizalde A, Eden C (2017) An evaluation of the North Sea circulation in global and regional models relevant for ecosystem simulations. Ocean Model 116:70–95. <https://doi.org/10.1016/j.ocemod.2017.06.005>

104. Eliassen SK, Hátún H, Larsen KMH, Hansen B, Rasmussen TAS (2017) Phenologically distinct phytoplankton regions on the Faroe Shelf - identified by satellite data, in-situ observations and model. *J Mar Syst* 169:99–110. <https://doi.org/10.1016/j.jmarsys.2017.01.015>
105. ICES (2019) Report of the Herring Assessment Working Group for the Area South of 62°N (HAWG). *ICES Sci Rep* 1(2):971. www.ices.dk
106. Coulson JC (2011) *The Kittiwake*. T & AD Poyser, London, pp 1–299
107. Eliassen K, Reinert J, Gaard E, Hansen B, Jacobsen JA, Grønkjær P, Christensen JT (2011) Sandeel as a link between primary production and higher trophic levels on the Faroe Shelf. *Mar Ecol Ser* 438:185–194. <https://doi.org/10.3354/meps09301>
108. Hansen B, Eliassen SK, Gaard E, Larsen KMH (2005) Climatic effects on plankton and productivity on the Faroe Shelf. *ICES J Mar Sci* 62:1224–1232. <https://doi.org/10.1016/j.icesjms.2005.04.014>
109. Steingrund P, Gaard E (2005) Relationship between phytoplankton production and cod production on the Faroe Shelf. *ICES J Mar Sci* 62:163–176. <https://doi.org/10.1016/j.icesjms.2004.08.019>
110. Gaard E, Hansen B, Heinesen SP (1998) Phytoplankton variability on the Faroe Shelf. *ICES J Mar Sci* 55:688–696. <https://doi.org/10.1006/jmsc.1998.0373>
111. Eliassen SK, Gaard E, Hansen B, Larsen KMH (2005) A ‘horizontal Sverdrup mechanism’ may control the spring bloom around small oceanic islands and over banks. *J Mar Syst* 56:352–362. <https://doi.org/10.1016/j.jmarsys.2005.03.005>
112. Gaard E (2003) Plankton variability on the Faroe Shelf during the 1990s. *ICES Mar Sci Symp* 219:182–189
113. Eliassen SK, Hansen B, Larsen KMH, Hátún H (2016) The exchange of water between the Faroe Shelf and the surrounding waters and its effect on the primary production. *J Mar Syst* 153:1–9. <https://doi.org/10.1016/j.jmarsys.2015.08.004>
114. Larsen KMH, Hansen B, Svendsen H (2008) Faroe shelf water. *Cont Shelf Res* 28:1754–1768. <https://doi.org/10.1016/j.csr.2008.04.006>
115. Bleck R (2002) An oceanic general circulation model framed in hybrid isopycnic-Cartesian coordinates. *Ocean Model* 4:55–88. [https://doi.org/10.1016/S1463-5003\(01\)00012-9](https://doi.org/10.1016/S1463-5003(01)00012-9)
116. Rasmussen TAS, Olsen SM, Hansen B, Hátún H, Larsen KMH (2014) The Faroe shelf circulation and its potential impact on the primary production. *Cont Shelf Res* 88:171–184. <https://doi.org/10.1016/j.csr.2014.07.014>
117. Holt J, Wakelin S, Huthnance J (2009) Down-welling circulation of the northwest European continental shelf: a driving mechanism for the continental shelf carbon pump. *Geophys Res Lett* 36:L14602. <https://doi.org/10.1029/2009GL038997>
118. Eliassen SK, Hátún H, Larsen KMH, Vang HBM, Rasmussen TAS (2019) The Faroe shelf spring bloom onset explained by a ‘critical volume hypothesis’. *J Mar Syst* 194:91–101. <https://doi.org/10.1016/j.jmarsys.2019.02.005>
119. Brzezinski MA (1985) The Si:C:N ration of marine diatoms: interspecific variability and the effect of some environmental variables. *J Phycol* 21:347–357. <https://doi.org/10.1111/j.0022-3646.1985.00347.x>
120. Djurhuus A, Jørgensen J, Hátún H, Debes HH, Christiansen DH (2015) Seasonal progression of microbial communities on the Faroe shelf. *Mar Biol Res* 11:895–908. <https://doi.org/10.1080/17451000.2015.1041532>
121. Hátún H, Larsen KMH, Debes H (2013) The western region. Technical report No 13-07, Faroe Marine Research Institute, 52p. <http://www.hav.fo/PDF/Ritgerdir/2013/TecRep1307.pdf>
122. Debes H, Gaard E, Hansen B (2008) Primary production on the Faroe shelf: temporal variability and environmental influences. *J Mar Syst* 74:686–697. <https://doi.org/10.1016/j.jmarsys.2008.07.004>
123. Jacobsen S, Gaard E, Larsen KMH, Eliassen SK, Hátún H (2018) Temporal and spatial variability of zooplankton on the Faroe shelf in spring 1997–2016. *J Mar Syst* 177:28–38. <https://doi.org/10.1016/j.jmarsys.2017.08.004>